

Accounting for statistical non-additive interactions enables the recovery of missing heritability from GWAS summary statistics

Samuel Pattillo Smith^{1-4,*}, Gregory Darnell^{1,5,*}, Dana Udwin⁶, Arbel Harpak^{3,4}, Sohini Ramachandran^{1,2,7,§}, and Lorin Crawford^{1,6,8,§,†}

1 Center for Computational Molecular Biology, Brown University, Providence, RI, USA

2 Department of Ecology and Evolutionary Biology, Brown University, Providence, RI, USA

3 Department of Integrative Biology, University of Texas at Austin, Austin, TX, USA

4 Department of Population Health, University of Texas at Austin, Austin, TX, USA

5 Institute for Computational and Experimental Research in Mathematics, Brown University, Providence, RI, USA

6 Department of Biostatistics, Brown University, Providence, RI, USA

7 Data Science Initiative, Brown University, Providence, RI, USA

8 Microsoft Research New England, Cambridge, MA, USA

*** Authors Contributed Equally**

§ Authors Contributed Equally

† Corresponding E-mail: lcrawford@microsoft.com

Abstract

LD score regression (LDSC) is a method to estimate narrow-sense heritability from genome-wide association study (GWAS) summary statistics alone, making it a fast and popular approach. The key concept underlying the LDSC framework is that there is a positive linear relationship between the magnitude of GWAS allelic effect estimates and linkage disequilibrium (LD) when complex traits are generated under the infinitesimal model — that is, causal variants are uniformly distributed along the genome and each have the same expected contribution to phenotypic variation. We present interaction-LD score (i-LDSC) regression: an extension of the original LDSC framework that accounts for non-additive genetic effects. By studying a wide range of generative models in simulations, and by re-analyzing 25 well-studied

28 quantitative phenotypes from 349,468 individuals in the UK Biobank and up to 159,095 individuals
29 in BioBank Japan, we show that the inclusion of a *cis*-interaction score (i.e., interactions between a
30 focal variant and nearby variants) significantly recovers substantial non-additive heritability that is not
31 captured by LDSC. For each of the 25 traits analyzed in the UK Biobank and 23 of the 25 traits analyzed
32 in BioBank Japan, *i*-LDSC detects a significant amount of variation contributed by genetic interactions.
33 The *i*-LDSC software and its application to these biobanks represent a step towards resolving further
34 genetic contributions of sources of non-additive genetic effects to complex trait variation.

35 Introduction

36 Heritability is defined as the proportion of phenotypic trait variation that can be explained by genetic
37 effects¹⁻³. Until recently, studies of heritability in humans have been reliant on typically small sized family
38 studies with known relatedness structures among individuals^{4,5}. Due to advances in genomic sequencing
39 and the steady development of statistical tools, it is now possible to obtain reliable heritability estimates
40 from biobank-scale data sets of unrelated individuals^{1,3,6,7}. Computational and privacy considerations
41 with genome-wide association studies (GWAS) in these larger cohorts have motivated a recent trend
42 to estimate heritability using summary statistics (i.e., estimated effect sizes and their corresponding
43 standard errors). In the GWAS framework, additive effect sizes and standard errors for individual single
44 nucleotide polymorphisms (SNPs) are estimated by regressing phenotype measurements onto the allele
45 counts of each SNP independently. Through the application of this approach over the last two decades,
46 it has become clear that many traits have a complex and polygenic basis—that is, hundreds to thousands
47 of individual genetic loci across the genome often contribute to the genetic basis of variation in a single
48 trait⁸.

49 Many statistical methods have been developed to improve the estimation of heritability from GWAS
50 summary statistics^{1,3,9,10}. The most widely used of these approaches is linkage disequilibrium (LD)
51 score regression and the corresponding LDSC software¹, which corrects for inflation in GWAS summary
52 statistics by modeling the relationship between the variance of SNP-level effect sizes and the sum of
53 correlation coefficients between focal SNPs and their genomic neighbors (i.e., the LD score of each variant).
54 The formulation of the LDSC framework relies on the fact that the expected relationship between chi-
55 square test statistics (i.e., the squared magnitude of GWAS allelic effect estimates) and LD scores holds

56 when complex traits are generated under the infinitesimal (or polygenic) model which assumes: (i) all
57 causal variants have the same expected contribution to phenotypic variation and (ii) causal variants are
58 uniformly distributed along the genome. Importantly, the estimand of the LDSC model is the proportion
59 of phenotypic variance attributable to additive effects of genotyped SNPs. The main motivation behind
60 the LDSC model is that, for polygenic traits, many marker SNPs tag nonzero effects. This may simply
61 arise because some of these SNPs are in LD with causal variants¹ or because their statistical association
62 is the product of a confounding factor such as population stratification.

63 As of late, there have been many efforts to build upon and improve the LDSC framework. For example,
64 recent work has shown that it is possible to estimate the proportion of phenotypic variation explained
65 by dominance effects¹¹ and local ancestry¹² using extensions of the LDSC model. One limitation of
66 LDSC is that, in practice, it only uses the diagonal elements of the squared LD matrix in its formulation
67 which, while computationally efficient, does not account for information about trait architecture that is
68 captured by the off-diagonal elements. This tradeoff helps LDSC to scale genome-wide, but it has also
69 been shown to lead to heritability estimates with large standard error^{10,13,14}. Recently, newer approaches
70 have attempted to reformulate the LDSC model by using the eigenvalues of the LD matrix to leverage
71 more of the information present in the correlation structure between SNPs^{3,10}.

72 In this paper, we show that the LDSC framework can be extended to estimate greater proportions
73 of genetic variance in complex traits (i.e., beyond the variance that is attributable to additive effects)
74 when a subset of causal variants are involved in a gene-by-gene ($G \times G$) interaction. Indeed, recent
75 association mapping studies have shown that $G \times G$ interactions can drive heterogeneity of causal variant
76 effect sizes¹⁵. Importantly, non-additive genetic effects have been proposed as one of the main factors
77 that explains “missing” heritability—the proportion of heritability not explained by the additive effects
78 of variants¹⁶.

79 The key insight we highlight in this manuscript is that SNP-level GWAS summary statistics can pro-
80 vide evidence of non-additive genetic effects contributing to trait architecture if there is a nonzero correla-
81 tion between individual-level genotypes and their statistical interactions. We present the “interaction-LD
82 score” regression model or *i*-LDSC: an extension of the LDSC framework which recovers “missing” heri-
83 tability by leveraging this “tagged” relationship between linear and nonlinear genetic effects. To validate
84 the performance of *i*-LDSC in simulation studies, we focus on synthetic trait architectures that have
85 been generated with contributions stemming from second-order and *cis*-acting statistical SNP-by-SNP

86 interaction effects; however, note that the general concept underlying *i*-LDSC can easily be extended to
87 other sources of non-additive genetic effects (e.g., gene-by-environment interactions). The main difference
88 between *i*-LDSC and LDSC is that the *i*-LDSC model includes an additional set of “*cis*-interaction” LD
89 scores in its regression model. These scores measure the amount of phenotypic variation contributed by
90 genetic interactions that can be explained by additive effects. In practice, these additional scores are
91 efficient to compute and require nothing more than access to a representative pairwise LD map, same as
92 the input required for LD score regression.

93 Through extensive simulations, we show that *i*-LDSC recovers substantial non-additive heritability
94 that is not captured by LDSC when genetic interactions are indeed present in the generative model for a
95 given complex trait. More importantly, *i*-LDSC has a calibrated type I error rate and does not overes-
96 timate non-additive genetic contributions to trait variation in simulated data when only additive effects
97 are present. While analyzing 25 complex traits in the UK Biobank and BioBank Japan, we illustrate
98 that pairwise interactions are a significant source of “missing” heritability captured by additive GWAS
99 summary statistics—suggesting that phenotypic variation due to non-additive genetic effects is more
100 pervasive in human phenotypes than previously reported. Specifically, we find evidence of significant
101 tagged non-additive genetic effects contributing to heritability estimates in all of the 25 traits in the
102 UK Biobank, and 23 of the 25 traits we analyzed in the BioBank Japan. We believe that *i*-LDSC, with
103 our development of a new *cis*-interaction score, represents a significant step towards resolving the true
104 contribution of genetic interactions.

105 Results

106 Overview of the interaction-LD score regression model

107 Interaction-LD score regression (*i*-LDSC) is a statistical framework for estimating heritability (i.e., the
108 proportion of trait variance attributable to genetic variance). Here, we will give an overview of the
109 *i*-LDSC method and its corresponding software, as well as detail how its underlying model differs from
110 that of LDSC¹. We will assume that we are analyzing a GWAS data set $\mathcal{D} = \{\mathbf{X}, \mathbf{y}\}$ where \mathbf{X} is an $N \times J$
111 matrix of genotypes with J denoting the number of SNPs (each of which is encoded as $\{0, 1, 2\}$ copies of
112 a reference allele at each locus j) and \mathbf{y} is an N -dimensional vector of measurements of a quantitative
113 trait. The *i*-LDSC framework only requires summary statistics of individual-level data: namely, marginal

114 effect size estimates for each SNP $\hat{\beta}$ and a sample LD matrix \mathbf{R} (which can be provided via reference
115 panel data).

116 We begin by assuming the following generative linear model for complex traits

$$117 \quad \mathbf{y} = \mu + \mathbf{X}\boldsymbol{\beta} + \mathbf{W}\boldsymbol{\theta} + \boldsymbol{\varepsilon}, \quad \boldsymbol{\varepsilon} \sim \mathcal{N}(\mathbf{0}, (1 - H^2)\mathbf{I}), \quad (1)$$

118 where μ is an intercept term; $\boldsymbol{\beta} = (\beta_1, \dots, \beta_J)$ is a J -dimensional vector containing the true additive effect
119 sizes for an additional copy of the reference allele at each locus on \mathbf{y} ; \mathbf{W} is an $N \times M$ matrix of (pairwise)
120 *cis*-acting SNP-by-SNP statistical interactions between some subset of causal SNPs, where columns of
121 this matrix are assumed to be the Hadamard (element-wise) product between genotypic vectors of the
122 form $\mathbf{x}_j \circ \mathbf{x}_k$ for the j -th and k -th variants; $\boldsymbol{\theta} = (\theta_1, \dots, \theta_M)$ is an M -dimensional vector containing
123 the interaction effect sizes; $\boldsymbol{\varepsilon}$ is a normally distributed error term with mean zero and variance scaled
124 according to the proportion of phenotypic variation not explained by genetic effects¹⁷, which we will
125 refer to as the broad-sense heritability of the trait denoted by H^2 ; and \mathbf{I} denotes an $N \times N$ identity
126 matrix. For convenience, we will assume that the genotype matrix (column-wise) and the trait of interest
127 have been mean-centered and standardized. Lastly, we let each individual effect size follow a Gaussian
128 distribution with variances proportional to their individual contributions to the heritability of the trait
129 of interest¹⁷⁻²¹

$$130 \quad \beta_j \sim \mathcal{N}(0, H^2 \rho / J), \quad \theta_m \sim \mathcal{N}(0, H^2 (1 - \rho) / M) \quad (2)$$

131 where ρ measures the proportion of total genetic effects that is contributed by additive genetic effects.
132 Effectively, we say $\mathbb{V}[\mathbf{X}\boldsymbol{\beta}] = H^2 \rho$ is the proportion of phenotypic variation contributed by additive SNP
133 effects under the generative model, while $\mathbb{V}[\mathbf{W}\boldsymbol{\theta}] = H^2 (1 - \rho)$ makes up the remaining proportion of
134 phenotypic variation contributed by genetic interactions.

135 A central objective in GWAS studies is to infer how much phenotypic variation can be explained
136 by genetic effects. To achieve that objective, a key consideration involves incorporating the possibility
137 of non-additive sources of genetic variation to be correlated with and explained by additive effect size
138 estimates obtained from GWAS analyses²². If we assume that the genotype and interaction matrices \mathbf{X}
139 and \mathbf{W} are not completely orthogonal (i.e., such that $\mathbf{X}^\top \mathbf{W} \neq \mathbf{0}$) then the following relationship between
140 the moment matrix $\mathbf{X}^\top \mathbf{y}$, the observed marginal GWAS summary statistics $\hat{\beta}$, and the true coefficient

141 values β from the generative model in Eq. (1) holds in expectation (see Materials and Methods)

$$142 \quad \mathbf{X}^\top \mathbf{y} = (\mathbf{X}^\top \mathbf{X})\beta + (\mathbf{X}^\top \mathbf{W})\theta \quad \stackrel{\approx}{\iff} \quad \hat{\beta} = \mathbf{R}\beta + \mathbf{V}\theta \quad (3)$$

143 where \mathbf{R} is a sample estimate of the LD matrix, and \mathbf{V} represents a sample estimate of the correlation
 144 between the individual-level genotypes \mathbf{X} and the span of genetic interactions between causal SNPs in \mathbf{W} .
 145 Intuitively, the term $\mathbf{V}\theta$ can be interpreted as the non-additive effects that are tagged by the additive
 146 effect estimates from the GWAS study. Note that, when (i) non-additive genetic effects play a negligible
 147 role on the overall architecture of a trait (i.e., such that $\theta = \mathbf{0}$) or (ii) the genotype and interaction
 148 matrices \mathbf{X} and \mathbf{W} do not share the same column space (i.e., such that $\mathbf{X}^\top \mathbf{W} = \mathbf{0}$), the equation above
 149 simplifies to a relationship between LD and summary statistics that is assumed in many GWAS studies
 150 and methods^{23–29}.

151 The goal of i-LDSC is to increase estimates of genetic variance by accounting for sources of non-additive
 152 genetic effects that can be explained by additive GWAS summary statistics. To do this, we extend the LD
 153 score regression framework and the corresponding LDSC software¹⁷. Here, according to Eq. (3), we note
 154 that $\hat{\beta} \sim \mathcal{N}(\mathbf{R}\beta + \mathbf{V}\theta, \lambda\mathbf{R})$ where λ is a scale variance term due to uncontrolled confounding effects^{10,30}.
 155 Next, we condition on $\Theta = (\beta, \theta)$ and take the expectation of chi-square statistics $\chi^2 = N\hat{\beta}\hat{\beta}^\top$ to yield

$$\begin{aligned} \mathbb{E}[\hat{\beta}\hat{\beta}^\top] &= \mathbb{E} \left[\mathbb{E} \left[\hat{\beta}\hat{\beta}^\top \mid \Theta \right] \right] = \mathbb{E} \left[\mathbb{V} \left[\hat{\beta} \mid \Theta \right] + \mathbb{E} \left[\hat{\beta} \mid \Theta \right] \mathbb{E} \left[\hat{\beta} \mid \Theta \right]^\top \right] \\ &= \mathbb{E} [\lambda\mathbf{R} + (\mathbf{R}\beta + \mathbf{V}\theta)(\mathbf{R}\beta + \mathbf{V}\theta)^\top] \\ 156 \quad &= \mathbb{E} [\lambda\mathbf{R} + \mathbf{R}\beta\beta^\top\mathbf{R} + 2\mathbf{R}\beta\theta^\top\mathbf{V} + \mathbf{V}\theta\theta^\top\mathbf{V}^\top] \\ &= \lambda\mathbf{R} + \left(\frac{H^2\rho}{J} \right) \mathbf{R}^2 + \left(\frac{H^2(1-\rho)}{M} \right) \mathbf{V}^2. \end{aligned} \quad (4)$$

157 We define $\ell_j = \sum_k r_{jk}^2$ as the LD score for the additive effect of the j -th variant¹⁷, and $f_j = \sum_m v_{jm}^2$
 158 represents the “*cis*-interaction” LD score which encodes the interaction between the j -th variant and
 159 all other variants within a genomic window that is a pre-specified number of SNPs wide²¹, respectively.
 160 By considering only the diagonal elements of LD matrix in the first term, similar to the original LDSC
 161 approach^{10,17}, we get the following simplified regression model

$$162 \quad \mathbb{E}[\chi^2] \propto \mathbf{1} + \ell\tau + f\sigma \quad (5)$$

163 where $\chi^2 = (\chi_1^2, \dots, \chi_J^2)$ is a J -dimensional vector of chi-square summary statistics, and $\ell = (\ell_1, \dots, \ell_J)$
164 and $\mathbf{f} = (f_1, \dots, f_J)$ are J -dimensional vectors of additive and *cis*-interaction LD scores, respectively.
165 Furthermore, we define the variance components $\tau = NH^2\rho/J$ and $\sigma = NH^2(1 - \rho)/M$ as the additive
166 and interaction regression coefficients of the model, and $\mathbf{1}$ is the intercept meant to model the bias factor
167 due to uncontrolled confounding effects (e.g., cryptic relatedness structure). In practice, we efficiently
168 compute the *cis*-interaction LD scores by considering only a subset of interactions between each j -th
169 focal SNP and SNPs within a *cis*-proximal window around the j -th SNP. In our validation studies and
170 applications, we base the width of this window on the observation that LD decays outside of a window
171 of 1 centimorgan (cM); therefore, SNPs outside the 1 cM window centered on the j -th SNP will not
172 significantly contribute to its LD scores. Note that the width of this window can be relaxed in the
173 i-LDSC software when appropriate. We fit the i-LDSC model using weighted least squares to estimate
174 regression parameters and derive P -values for identifying traits that have significant statistical evidence
175 of tagged *cis*-interaction effects by testing the null hypothesis $H_0 : \sigma = NH^2(1 - \rho)/M = 0$. Importantly,
176 under the null model of a trait being generated by only additive effects, the i-LDSC model in Eq. (5)
177 reduces to the infinitesimal model³¹.

178 Lastly, we want to note the empirical observation that the additive (ℓ) and interaction (\mathbf{f}) LD scores
179 are lowly correlated. This is important because it indicates that the presence of *cis*-interaction LD scores
180 in the model specified in Eq. (5) has little-to-no influence over the estimate for the additive coefficient
181 τ . Instead, the inclusion of \mathbf{f} creates a multivariate model that can identify the proportion of variance
182 explained by both additive and non-additive effects in summary statistics. In other words, we can
183 interpret σ as the phenotypic variation explained by tagged *cis*-acting interaction effects, and we use the
184 sum of coefficient estimates $\hat{\tau} + \hat{\sigma}$ to construct i-LDSC heritability estimates. A full derivation of the
185 *cis*-interaction regression framework and details about its corresponding implementation in our software
186 i-LDSC can be found in Materials and Methods.

187 **Detection of tagged non-additive effects using i-LDSC in simulations**

188 We illustrate the power of i-LDSC across different genetic trait architectures via extensive simulation
189 studies (Materials and Methods). We generate synthetic phenotypes using real genome-wide genotype
190 data from individuals of self-identified European ancestry in the UK Biobank. To do so, we first assume
191 that traits have a polygenic architecture where all SNPs have a nonzero additive effect. Next, we randomly

192 select a set of causal *cis*-interaction variants and divide them into two interacting groups (Materials and
193 Methods). One may interpret the SNPs in group #1 as being the “hubs” in an interaction map²¹; while,
194 SNPs in group #2 are selected to be variants within some kilobase (kb) window around each SNP in
195 group #1. We assume a wide range of simulation scenarios by varying the following parameters:

- 196 • heritability: $H^2 = 0.3$ and 0.6 ;
- 197 • proportion of phenotypic variation that is generated by additive effects: $\rho = 0.5, 0.8,$ and 1 ;
- 198 • percentage of SNPs selected to be in group #1: $1\%, 5\%,$ and 10% ;
- 199 • genomic window used to assign SNPs to group #2: ± 10 and ± 100 kb.

200 We also varied the correlation between SNP effect size and minor allele frequency (MAF) (as discussed
201 in Schoech et al.³²). All results presented in this section are based on 100 different simulated phenotypes
202 for each parameter combination.

203 Figure 1 demonstrates that i-LDSC robustly detects significant tagged non-additive genetic variance,
204 regardless of the total number of causal interactions genome-wide. Instead, the power of i-LDSC depends
205 on the proportion of phenotypic variation that is generated by additive versus interaction effects (ρ), and
206 its power tends to scale with the window size used to compute the *cis*-interaction LD scores (see Materials
207 and Methods). i-LDSC shows a similar performance for detecting tagged *cis*-interaction effects when the
208 effect sizes of causal SNPs depend on their minor allele frequency and when we varied the number of
209 SNPs assigned to be in group #2 within 10 kb and 100kb windows, respectively (Figures S1-S5).

210 Importantly, i-LDSC does not falsely identify putative non-additive genetic effects in GWAS summary
211 statistics when the synthetic phenotype was generated by only additive effects ($\rho = 1$). Figure 2 illustrates
212 the performance of i-LDSC under the null hypothesis $H_0 : \sigma = NH^2(1 - \rho)/M = 0$, with the type I error
213 rates for different estimation window sizes of the *cis*-interaction LD scores highlighted in panel A. Here,
214 we also show that, when no genetic interaction effects are present, i-LDSC unbiasedly estimates the
215 *cis*-interaction coefficient in the regression model $\sigma = 0$ (Figure 2B), robustly estimates the heritability
216 (Figure 2C), and provides well-calibrated *P*-values when assessed over many traits (Figure 2D). This
217 behavior is consistent across different MAF-dependent effect size distributions, and *P*-value calibration is
218 not sensitive to misspecification of the estimation windows used to generate the *cis*-interaction LD scores
219 (Figures S6-S7).

220 One of the innovations that *i*-LDSC offers over the traditional LDSC framework is increased heritabil-
221 ity estimates after the identification of non-additive genetic effects that are tagged by GWAS summary
222 statistics. Here, we applied both methods to the same set of simulations in order to understand how
223 LDSC behaves for traits generated with *cis*-interaction effects. Figure 3 depicts boxplots of the heri-
224 tability estimates for each approach and shows that, across an array of different synthetic phenotype
225 architectures, LDSC captures less of phenotypic variance explained by all genetic effects. It is important
226 to note that *i*-LDSC can yield upwardly biased heritability estimates when the *cis*-interaction scores are
227 computed over genomic window sizes that are too small; however, these estimates become more accurate
228 for larger window size choices (Figure S8). In contrast to LDSC, which aims to capture phenotypic variance
229 attributable to the additive effects of genotyped SNPs, *i*-LDSC accurately partitions genetic effects into
230 additive versus *cis*-interacting components, which in turn generally leads the ability of *i*-LDSC to capture
231 more genetic variance. The mean absolute error between the true generative heritability and heritability
232 estimates produced by *i*-LDSC and LDSC are shown in Tables S1 and S2, respectively. Generally, the
233 error in heritability estimates is higher for LDSC than it is for *i*-LDSC across each of the scenarios that
234 we consider.

235 Lastly, we perform an additional set of simulations where we explore other common generative mod-
236 els for complex trait architecture that involve non-additive genetic effects. Specifically, we compare
237 heritability estimates from LDSC and *i*-LDSC in the presence of additive effects, *cis*-acting interactions,
238 and a third source of genetic variance stemming from either gene-by-environment ($G \times E$) or or gene-
239 by-ancestry ($G \times \text{Ancestry}$) effects. Details on how these components were generated can be found in
240 Materials and Methods. In general, *i*-LDSC underestimates overall heritability when additive effects and
241 *cis*-acting interactions are present alongside $G \times E$ (Figure S9) and/or $G \times \text{Ancestry}$ effects when PCs are
242 included as covariates (Figure S10). Notably, when PCs are not included to correct for residual stratifica-
243 tion, both LDSC and *i*-LDSC can yield unbounded heritability estimates greater than 1 (Figure S11). Also
244 interestingly, when we omit *cis*-interactions from the generative model (i.e., the genetic architecture of
245 simulated traits is only made up of additive and $G \times E$ or $G \times \text{Ancestry}$ effects), *i*-LDSC will still estimate
246 a nonzero genetic variance component with the *cis*-interaction LD scores (Figures S12-S14). Collectively,
247 these results empirically show the important point that *cis*-interaction scores are not enough to recover
248 missing genetic variation for all types of trait architectures; however, they are helpful in recovering pheno-
249 typic variation explained by statistical *cis*-interaction effects. Recall that the linear relationship between

(expected) χ^2 test statistics and LD scores proposed by the LDSC framework holds when complex traits are generated under the polygenic model where all causal variants have the same expected contribution to phenotypic variation. When *cis*-interactions affect genetic architecture (e.g., in our earlier simulations in Figure 3), these assumptions are violated in LDSC, but the inclusion of the additional nonlinear scores in i-LDSC help recover the relationship between the expectation of χ^2 test statistics and LD.

As a final demonstration of how i-LDSC performs when assumptions of the original LD score model are violated, we also generated synthetic phenotypes with sparse architectures using the spike-and-slab model²⁰. Here, traits were simulated with solely additive effects, but this time only variants with the top or bottom {1, 5, 10, 25, 50, 100} percentile of LD scores were given nonzero effects (see Material and Methods). Breaking the relationship assumed under the LDSC framework between LD scores and chi-squared statistics (i.e., that they are generally positively correlated) led to unbounded estimates of heritability in all but the (polygenic) scenario when 100% of SNPs contributed to the phenotypic variation (Figure S15).

Application of i-LDSC to the UK Biobank and BioBank Japan

To assess whether non-additive genetic effects are significantly affecting estimates of heritability in empirical biobank data, we applied i-LDSC to 25 continuous quantitative traits from the UK Biobank and BioBank Japan (Table S3). Protocols for computing GWAS summary statistics for the UK Biobank are described in the Materials and Methods; while pre-computed summary statistics for BioBank Japan were downloaded directly from the consortium website (see URLs). We release the *cis*-acting SNP-by-SNP interaction LD scores used in our analyses on the i-LDSC GitHub repository from two reference groups in the 1000 Genomes: 489 individuals from the European superpopulation (EUR) and 504 individuals from the East Asian (EAS) superpopulation (see also Table S4).

In each of the 25 traits we analyzed in the UK Biobank, we detected significant proportions of estimated genetic variation stemming from tagged pairwise *cis*-interactions (Table 1). This includes many canonical traits of interest in heritability analyses: height, cholesterol levels, urate levels, and both systolic and diastolic blood pressure. Our findings in Table 1 are supported by multiple published studies identifying evidence of non-additive effects playing a role in the architectures of different traits of interest. For example, Li et al.³³ found evidence for genetic interactions that contributed to the pathogenesis of coronary artery disease. It was also recently shown that non-additive genetic effects plays a significant

279 role in body mass index¹⁰. Generally, we find that the traditional LDSC produces lower estimates of
280 trait heritability because it does not consider the additional sources of genetic signal that i-LDSC does
281 (Table 1). In BioBank Japan, 23 of the 25 traits analyzed had a significant nonlinear component detected
282 by i-LDSC — with HDL and triglyceride levels being the only exceptions. We performed an additional
283 analysis where the *cis*-interaction scores are included as an annotation alongside 97 other functional
284 categories in the stratified-LD score regression framework and its software s-LDSC³⁴ (Materials and
285 Methods). Here, s-LDSC heritability estimates still showed an increase with the interaction scores versus
286 when the publicly available functional categories were analyzed alone (Table S6).

287 For each of the 25 traits that we analyzed, we found that the i-LDSC heritability estimates are
288 significantly correlated with corresponding estimates from LDSC in both the UK Biobank ($r^2 = 0.988$,
289 $P = 5.936 \times 10^{-24}$) and BioBank Japan ($r^2 = 0.849$, $P = 6.061 \times 10^{-11}$) as shown in Figure 4A.
290 Additionally, we found that the heritability estimates for the same traits between the two biobanks are
291 highly correlated according to both LDSC ($r^2 = 0.848$, $P = 7.166 \times 10^{-11}$) and i-LDSC ($r^2 = 0.666$,
292 $P = 6.551 \times 10^{-7}$) analyses as shown in Figure 4B.

293 After comparing the i-LDSC heritability estimates to LDSC, we then assessed whether there was sig-
294 nificant difference in the amount of phenotypic variation explained by the non-additive genetic effect
295 component in the GWAS summary statistics derived from the the UK Biobank and BioBank Japan (i.e.,
296 comparing the estimates of σ ; see Figure 4C). We show that, while heterogeneous between traits, the phe-
297 notypic variation explained by genetic interactions is relatively of the same magnitude for both biobanks
298 ($r^2 = 0.372$, $P = 0.0119$). Notably, the trait with the most significant evidence of tagged *cis*-interaction
299 effects in GWAS summary statistics is height which is known to have a highly polygenic architecture.

300 Finally, we show that the intercepts estimated by LDSC and i-LDSC are highly correlated in both the
301 UK Biobank and the BioBank Japan (Figure 4D). Recall that these intercept estimates represent the
302 confounding factor due to uncontrolled effects. For LDSC, this does include phenotypic variation that is
303 due to unaccounted for pairwise statistical genetic interactions. The i-LDSC intercept estimates tend to
304 be correlated with, but are generally different than, those computed with LDSC — empirically indicating
305 that non-additive genetic variation is partitioned away and is missed when using the standard LD score
306 alone. This result shows similar patterns in both the UK Biobank ($r^2 = 0.888$, $P = 1.962 \times 10^{-12}$) and
307 BioBank Japan ($r^2 = 0.813$, $P = 7.814 \times 10^{-10}$), and it confirms that non-additive genetic effects can be
308 a source of “missing” phenotypic variance explained in heritability estimation.

309 Discussion

310 In this paper, we present *i*-LDSC, an extension of the LD score regression framework which aims to
311 recover missing heritability from GWAS summary statistics by incorporating an additional score that
312 measures the non-additive genetic variation that is tagged by genotyped SNPs. Here, we demonstrate how
313 *i*-LDSC builds upon the original LDSC model through the development of new “*cis*-interaction” LD scores
314 which help to investigate signals of *cis*-acting SNP-by-SNP interactions (Figures 1 and S1-S5). Through
315 extensive simulations, we show that *i*-LDSC is well-calibrated under the null model when polygenic traits
316 are generated only by additive effects (Figures 2 and S6-S7), and it provides greater heritability estimates
317 over LDSC when traits are indeed generated with *cis*-acting SNP-by-SNP interaction effects (Figures 3 and
318 S8, and Tables S1 and S2). Finally, in real data, we show examples of many traits with estimated GWAS
319 summary statistics that tag *cis*-interaction effects in the UK Biobank and BioBank Japan (Figures 4
320 and S16, and Tables 1 and S3-S6). We have made *i*-LDSC a publicly available command line tool that
321 requires minimal updates to the computing environment used to run the original implementation of LD
322 score regression (see URLs). In addition, we provide pre-computed *cis*-interaction LD scores calculated
323 from the European (EUR) and East Asian (EAS) reference populations in the 1000 Genomes phase 3
324 data (see Data and Software Availability under Materials and Methods).

325 The current implementation of the *i*-LDSC framework offers many directions for future development
326 and applications. First, as we showed with our simulation studies (Figures S9-S15), the *cis*-interaction
327 LD scores that we propose are not always enough to recover explainable non-additive genetic effects for all
328 types of trait architectures. While we focus on pairwise *cis*-acting SNP-by-SNP statistical interactions in
329 this work, the theoretical concepts underlying *i*-LDSC can easily be adapted to other types of interactions
330 as well. Second, in our analysis of the UK Biobank and BioBank Japan, we showed that the inclusion
331 of additional categories via frameworks such as stratified LD score regression³⁵ can be used to provide
332 more refined heritability estimates from GWAS summary statistics while accounting for linkage (see
333 results in Table 1 versus Table S6). A key part of our future work is to continue to explore whether
334 considering functional annotation groups would also improve our ability to identify tagged non-additive
335 genetic effects. Lastly, we have only focused on analyzing one phenotype at a time in this study. However,
336 many previous studies have extensively shown that modeling multiple phenotypes can often dramatically
337 increase power^{36,37}. Therefore, it would be interesting to extend the *i*-LDSC framework to multiple traits

338 to study nonlinear genetic correlations in the same way that LDSC was recently extended to uncover
339 additive genetic correlation maps across traits³⁸.

340 URLs

341 i-LDSC software package for implementing interaction score regression, <https://github.com/lcrawlab/>
342 i-LDSC; LDSC software package for implementing LD score regression, <https://github.com/bulik/>
343 [ldsc/](https://github.com/bulik/ldsc/); UK Biobank, <https://www.ukbiobank.ac.uk>; BioBank Japan, <http://jenger.riken.jp/en/>
344 [result](http://jenger.riken.jp/en/result); 1000 Genomes Project genetic map and haplotypes, <http://mathgen.stats.ox.ac.uk/impute/>
345 [data_download_1000G_phase1_integrated.html](http://mathgen.stats.ox.ac.uk/impute/data_download_1000G_phase1_integrated.html); Database of Genotypes and Phenotypes (dbGaP),
346 <https://www.ncbi.nlm.nih.gov/gap>; NHGRI-EBI GWAS Catalog, <https://www.ebi.ac.uk/gwas/>;
347 GRM-MAF-LD package, <https://github.com/arminschoech/GRM-MAF-LD>; GCTA toolkit, [https://](https://yanglab.westlake.edu.cn/software/gcta/)
348 yanglab.westlake.edu.cn/software/gcta/.

349 Acknowledgements

350 We thank Jeffrey P. Spence, Roshni Patel, Matthew Aguirre, Mineto Ota, and our anonymous referees for
351 insightful comments on an earlier version of this manuscript as well as the Harpak, Ramachandran, and
352 Crawford Labs for helpful discussions. This research was conducted in part using computational resources
353 and services at the Center for Computation and Visualization at Brown University. This research was
354 also conducted using the UK Biobank Resource under Application Numbers 14649 (LC) and 22419 (SR).
355 S.P. Smith and D. Udwin were trainees supported under the Brown University Predoctoral Training
356 Program in Biological Data Science (NIH T32 GM128596). S.P. Smith was also supported by NIH
357 RF1AG073593. G. Darnell was supported by NSF Grant No. DMS-1439786 while in residence at the
358 Institute for Computational and Experimental Research in Mathematics (ICERM) in Providence, RI. This
359 research was supported in part by an Alfred P. Sloan Research Fellowship and a David & Lucile Packard
360 Fellowship for Science and Engineering awarded to L. Crawford. This research was also partly supported
361 by US National Institutes of Health (NIH) grant R01 GM118652, NIH grant R35 GM139628, and National
362 Science Foundation (NSF) CAREER award DBI-1452622 to S. Ramachandran. Any opinions, findings,
363 and conclusions or recommendations expressed in this material are those of the author(s) and do not

364 necessarily reflect the views of any of the funders.

365 **Author Contributions**

366 SPS, GD, SR, and LC conceived the study and developed the methods. SPS, GD, and LC developed
367 the algorithms and software. All authors performed the analyses, interpreted the results, and wrote and
368 revised the manuscript.

369 **Competing Interests**

370 The authors declare no competing interests.

371 **Materials and Methods**

372 **Generative statistical model for complex traits**

373 Our goal in this study is to re-analyze summary statistics from genome-wide association studies (GWAS)
374 and estimate heritability while accounting for both additive genetic associations and tagged interaction
375 effects. We begin by assuming the following generative linear model for complex traits and phenotypes

$$376 \quad \mathbf{y} = \mu + \mathbf{X}\boldsymbol{\beta} + \mathbf{W}\boldsymbol{\theta} + \boldsymbol{\varepsilon}, \quad \boldsymbol{\varepsilon} \sim \mathcal{N}(\mathbf{0}, (1 - H^2)\mathbf{I}), \quad (6)$$

377 where \mathbf{y} denotes an N -dimensional vector of phenotypic states for a quantitative trait of interest measured
378 in N individuals; μ is an intercept term; \mathbf{X} is an $N \times J$ matrix of genotypes, with J denoting the number
379 of single nucleotide polymorphism (SNPs) encoded as $\{0, 1, 2\}$ copies of a reference allele at each locus;
380 $\boldsymbol{\beta} = (\beta_1, \dots, \beta_J)$ is a J -dimensional vector containing the true additive effect sizes for an additional copy
381 of the reference allele at each locus on \mathbf{y} ; \mathbf{W} is an $N \times M$ matrix of genetic interactions; $\boldsymbol{\theta} = (\theta_1, \dots, \theta_M)$
382 is an M -dimensional vector containing the interaction effect sizes; $\boldsymbol{\varepsilon}$ is a normally distributed error term
383 with mean zero and variance scaled according to the proportion of phenotypic variation not explained by
384 the broad-sense heritability of the trait, denoted by H^2 ; and \mathbf{I} denotes an $N \times N$ identity matrix. While in
385 theory, the matrix \mathbf{W} could encode any source of non-additive genetic effects (e.g., gene-by-environmental
386 effects), we limit our focus in this study to trait architectures that have been generated with contributions
387 stemming from *cis*-acting statistical SNP-by-SNP interactions. To that end, we assume that the columns
388 of \mathbf{W} are the Hadamard (element-wise) product between genotypic vectors of the form $\mathbf{x}_j \circ \mathbf{x}_k$ for the
389 j -th and k -th variants.

390 For convenience, we further assume that the genotype matrix (column-wise) and trait of interest have
391 been mean-centered and standardized. Furthermore, we want to point out that the generative formulation
392 of Eq. (6) can also be easily extended to accommodate other fixed effects (e.g., age, sex, or genotype
393 principal components), as well as other random effects terms that can be used to account for sample
394 non-independence due to other environmental factors. In addition, we choose to assume that $\boldsymbol{\beta}$ and $\boldsymbol{\theta}$
395 are fixed effects here, but modeling these coefficients as a random effect is straightforward. Lastly, in this
396 work, we only consider second order (or pairwise) SNP-by-SNP interactions. However, the generalization
397 of the proposed framework to detect genetic effects from higher-order interactions is also straightforward

398 and only involves manipulating the interaction matrix \mathbf{W} ^{21,39}.

399 **GWA summary statistics and tagged interaction effects**

400 As previously mentioned, the key to this work is that SNP-level GWAS summary statistics can also
401 tag non-additive genetic effects if there is a nonzero correlation between individual-level genotypes and
402 their interactions (as defined in Eq. (6)). Throughout this section, we will use $\mathbf{X}^\top \mathbf{X}/N$ to denote the
403 linkage disequilibrium (LD) or pairwise correlation matrix between SNPs. We will then let \mathbf{R} represent
404 an LD matrix empirically estimated from external data (e.g., directly from GWAS study data, or using a
405 pairwise LD map from a population that is representative of the samples analyzed in the GWAS study).
406 The important property here is that

$$407 \quad \mathbb{E}[\mathbf{X}^\top \mathbf{X}] \approx N\mathbf{R}, \quad \mathbb{E}[\mathbf{x}_j^\top \mathbf{x}_j] \approx N, \quad \mathbb{E}[\mathbf{x}_j^\top \mathbf{x}_k] \approx Nr_{jk} \quad (7)$$

408 where the term r_{jk} is defined as the Pearson correlation coefficient between the j -th and k -th SNPs,
409 respectively, and \mathbf{x}_j denotes the j -th column of the individual-level genotype matrix \mathbf{X} .

410 A central goal in GWAS studies is to jointly infer how much phenotypic variation can be explained by
411 genetic effects. This often amounts to estimating the effect sizes $\boldsymbol{\beta} = (\mathbf{X}^\top \mathbf{X})^{-1} \mathbf{X}^\top \mathbf{y}$ for each SNP, given
412 both genotypic and phenotypic measurements for each assayed individual. However, since the generative
413 model in Eq. (6) is an underdetermined linear system (i.e., $J > N$) for many GWAS applications, we
414 need to make additional modeling assumptions on the regression coefficients to make the generative model
415 identifiable. To do so, we follow standard linear modeling approaches¹⁷⁻²¹ and assume that each effect
416 size follows a Gaussian distribution with variances proportional to their individual contributions to the
417 heritability of the trait of interest. Namely, we assume that

$$418 \quad \beta_j \sim \mathcal{N}(0, H^2 \rho / J), \quad \theta_m \sim \mathcal{N}(0, H^2 (1 - \rho) / M), \quad j = 1, \dots, J \quad m = 1, \dots, M \quad (8)$$

419 where ρ measures the proportion of total genetic effects that is contributed by the additive effects in the
420 generative model. Alternatively, we say that $\mathbb{V}[\mathbf{X}\boldsymbol{\beta}] = H^2 \rho$ is the proportion of phenotypic variation
421 contributed by additive SNP effects under the generative model, which then leaves the set of interactions
422 involving some subset of causal SNPs to contribute the remaining $\mathbb{V}[\mathbf{W}\boldsymbol{\theta}] = H^2 (1 - \rho)$ proportion to the

423 heritability.

424 **Traditional estimation of additive GWAS summary statistics**

425 In traditional GWAS studies, summary statistics of the true additive effects β in Eq. (6) are typically
426 derived by computing a marginal least squares estimate with the observed data

$$427 \quad \hat{\beta}_j = (\mathbf{x}_j^\top \mathbf{x}_j)^{-1} \mathbf{x}_j^\top \mathbf{y} \quad \iff \quad \hat{\beta} = \text{diag}(\mathbf{X}^\top \mathbf{X})^{-1} \mathbf{X}^\top \mathbf{y}. \quad (9)$$

428 There are two key identities that may be taken from Eq. (9). The first uses Eq. (7) and is the approximate
429 relationship (in expectation) between the moment matrix $\mathbf{X}^\top \mathbf{y}$ and the linear effect size estimates $\hat{\beta}$:

$$430 \quad \mathbf{X}^\top \mathbf{y} = \text{diag}(\mathbf{X}^\top \mathbf{X}) \hat{\beta} \approx N \hat{\beta}. \quad (10)$$

431 The second key point combines Eqs. (7) and (10) to describe the asymptotic relationship between the
432 observed marginal GWAS summary statistics $\hat{\beta}$ and the joint coefficient values β where

$$433 \quad \beta = (\mathbf{X}^\top \mathbf{X})^{-1} \mathbf{X}^\top \mathbf{y} \approx (NR)^{-1} N \hat{\beta} = \mathbf{R}^{-1} \hat{\beta}. \quad (11)$$

434 After some algebra, the above mirrors a high-dimensional regression model (in expectation) where $\hat{\beta} = \mathbf{R}\beta$
435 with the estimated summary statistics as the response variables and the empirically estimated LD matrix
436 acting as the design matrix^{23,26,28,29,40}. Theoretically, the resulting output coefficients from this high-
437 dimensional model are the desired true effect size estimates used to generate the phenotype of interest.

438 **Additive GWAS summary statistics with tagged interaction effects**

439 When interactions contribute to the architecture of complex traits (i.e., $\theta \neq \mathbf{0}$ and $\rho < 1$), the marginal
440 GWAS summary statistics derived using least squares in Eq. (9) can also explain non-additive variation
441 if there is a nonzero correlation between genotypes and their interactions. To see this, we take the joint
442 solution for the true regression coefficients β and θ from the generative model in Eq. (6)

$$443 \quad \begin{bmatrix} \beta \\ \theta \end{bmatrix} = \begin{bmatrix} \mathbf{X}^\top \mathbf{X} & \mathbf{X}^\top \mathbf{W} \\ \mathbf{W}^\top \mathbf{X} & \mathbf{W}^\top \mathbf{W} \end{bmatrix}^{-1} \begin{bmatrix} \mathbf{X}^\top \\ \mathbf{W}^\top \end{bmatrix} \mathbf{y}, \quad (12)$$

444 where the matrix $\mathbf{X}^T\mathbf{W}$ can be interpreted as the sample correlation between individual-level genotypes
445 and the *cis*-interactions between causal SNPs. By solving for the additive genetic effects (again in
446 expectation using Eqs. (7) and (10)), we get the following alternative relationship between the moment
447 matrix $\mathbf{X}^T\mathbf{y}$, the observed marginal GWAS summary statistics $\widehat{\boldsymbol{\beta}}$, and the true coefficient values $\boldsymbol{\beta}$ where

$$448 \quad \mathbf{X}^T\mathbf{y} = (\mathbf{X}^T\mathbf{X})\boldsymbol{\beta} + (\mathbf{X}^T\mathbf{W})\boldsymbol{\theta} \quad \Leftrightarrow \quad \widehat{\boldsymbol{\beta}} = \mathbf{R}\boldsymbol{\beta} + \mathbf{V}\boldsymbol{\theta}. \quad (13)$$

449 Here, we define \mathbf{V} to represent a sample estimate of the correlation between the individual-level genotypes
450 and the non-additive genetic interaction matrix such that $\mathbb{E}[\mathbf{X}^T\mathbf{W}] \approx N\mathbf{V}$. Similar to the LD matrix \mathbf{R} ,
451 the correlation matrix \mathbf{V} is also assumed to be computed from reference panel data. Intuitively, when
452 $\mathbf{V}\boldsymbol{\theta} \neq \mathbf{0}$ there is additional phenotypic variation contributed by genetic interactions that can be explained
453 by GWAS effect size estimates. Moreover, when $\mathbf{V}\boldsymbol{\theta} = \mathbf{0}$, then the relationship in Eq. (13) converges
454 onto the conventional asymptotic assumption (in expectation) between GWAS summary statistics and
455 the true additive coefficients in Eq. (11)^{23,26,28,29,40}.

456 Full derivation of interaction LD score regression

457 In order to derive the interaction LD score (i-LDSC) regression framework, recall that our goal is to
458 identify evidence of tagged interaction effects within GWAS summary statistics. To do this, we build
459 upon the LD score regression framework and the LDSC software¹⁷. Here, we assume nonzero contributions
460 from *cis*-acting SNP-by-SNP interaction effects in the generative model of complex traits as in Eq. (13),
461 and we use the observed least squares estimates from Eq. (9) to compute chi-square statistics $\chi_j^2 = N\widehat{\beta}_j^2$
462 for every $j = 1, \dots, J$ variant in the data. Taking the expectation of these statistics yields

$$463 \quad \mathbb{E}[\chi_j^2] = N\mathbb{E}[\widehat{\beta}_j^2] = N \left[\mathbb{V}[\widehat{\beta}_j] + \left(\mathbb{E}[\widehat{\beta}_j] \right)^2 \right]. \quad (14)$$

464 We can simplify Eq. (14) in two steps. First, by combining the prior assumption in Eq. (8) and the
465 asymptotic approximation in Eq. (13), we can show that marginal expectation (i.e., when not conditioning
466 on the true coefficients) $\mathbb{E}[\widehat{\beta}_j] = 0$ for all variants. Second, by conditioning on the generative model from

Eq. (6), we can use the law of total variance to simplify $\mathbb{V}[\widehat{\beta}_j]$ where

$$\begin{aligned} \mathbb{V}[\widehat{\beta}_j] &= \mathbb{E}[\mathbb{V}[\widehat{\beta}_j | \mathbf{X}]] + \mathbb{V}[\mathbb{E}[\widehat{\beta}_j | \mathbf{X}]] \approx \mathbb{E}[\mathbb{V}[\mathbf{x}_j^\top \mathbf{y} / N | \mathbf{X}]] + 0 \\ &= \mathbb{E} \left[\frac{1}{N^2} \mathbf{x}_j^\top \{ \mathbb{V}[\mathbf{y} | \mathbf{X}] \} \mathbf{x}_j \right] \\ &= \mathbb{E} \left[\frac{1}{N^2} \mathbf{x}_j^\top \left\{ \frac{H^2 \rho}{J} \mathbf{X} \mathbf{X}^\top + \frac{H^2(1-\rho)}{M} \mathbf{W} \mathbf{W}^\top + (1-H^2) \right\} \mathbf{x}_j \right] \\ &= \mathbb{E} \left[\frac{1}{N^2} \left\{ \frac{H^2 \rho}{J} \mathbf{x}_j^\top \mathbf{X} \mathbf{X}^\top \mathbf{x}_j + \frac{H^2(1-\rho)}{M} \mathbf{x}_j^\top \mathbf{W} \mathbf{W}^\top \mathbf{x}_j + N(1-H^2) \right\} \right]. \end{aligned}$$

Using the same logic from the original LDSC regression framework¹⁷, we can use Isserlis' theorem⁴¹ to write the above in terms of more familiar quantities based on sample correlations

$$\frac{1}{N^2} \mathbf{x}_j^\top \mathbf{X} \mathbf{X}^\top \mathbf{x}_j = \sum_{k=1}^J \widetilde{r}_{jk}^2, \quad \frac{1}{N^2} \mathbf{x}_j^\top \mathbf{W} \mathbf{W}^\top \mathbf{x}_j = \sum_{m=1}^M \widetilde{v}_{jm}^2 \quad (15)$$

where \widetilde{r}_{jk} is used to denote the sample correlation between additively-coded genotypes at the j -th and k -th variants, and \widetilde{v}_{jm} is used to denote the sample correlation between the genotype of the j -th variant and the m -th genetic interaction on the phenotype of interest (again see Eq. (13)). Furthermore, we can use the delta method (only displaying terms up to $\mathcal{O}(1/N^2)$) to show that (in expectation)

$$\mathbb{E}[\widetilde{r}_{jk}^2] \approx r_{jk}^2 + (1 - r_{jk}^2)/N, \quad \mathbb{E}[\widetilde{v}_{jm}^2] \approx v_{jm}^2 + (1 - v_{jm}^2)/N. \quad (16)$$

Next, we can then approximate the quantities in Eq. (15) via the following

$$\mathbb{E} \left[\sum_{k=1}^J \widetilde{r}_{jk}^2 \right] \approx \ell_j + (J - \ell_j)/N, \quad \mathbb{E} \left[\sum_{m=1}^M \widetilde{v}_{jm}^2 \right] \approx f_j + (M - f_j)/N \quad (17)$$

where ℓ_j is the corresponding LD score for the additive effect of the j -th variant and f_j represents the ‘‘interaction’’ LD score between the j -th SNP and all other variants in the data set²¹, respectively.

Altogether, this leads to the specification of the univariate framework with the j -th SNP

$$\mathbb{E}[\chi_j^2] \approx N \left[\left(\frac{H^2 \rho}{J} \right) \ell_j + \left(\frac{H^2(1-\rho)}{M} \right) f_j + \frac{1}{N} (1-H^2) \right] = \ell_j \tau + f_j \sigma + 1 \quad (18)$$

483 where we define $\tau = NH^2\rho/J$ as estimates of the additive genetic signal, the coefficient $\sigma = NH^2(1-\rho)/M$
484 as an estimate of the proportion of phenotypic variation explained by tagged interaction effects, and $\mathbf{1}$
485 is the intercept meant to model the misestimation due to uncontrolled confounding effects (e.g., cryptic
486 relatedness and population stratification). Similar to the original LDSC formulation, an intercept greater
487 than one means significant bias. Note that the simplification for many of the terms above such as
488 $(1 - H^2)/N \approx 1/N$ results from our assumption that the number of individuals in our study is large. For
489 example, the sample sizes for each biobank-scale study considered in the analyses of this manuscript are
490 at least on the order of $N \geq 10^4$ observations (see Table S5). Altogether, we can jointly express Eq. (18)
491 in multivariate form as

$$492 \quad \mathbb{E}[\chi^2] \approx \boldsymbol{\ell}\tau + \mathbf{f}\sigma + \mathbf{1} \quad (19)$$

493 where $\boldsymbol{\chi}^2 = (\chi_1^2, \dots, \chi_J^2)$ is a J -dimensional vector of chi-square summary statistics, and $\boldsymbol{\ell} = (\ell_1, \dots, \ell_J)$
494 and $\mathbf{f} = (f_1, \dots, f_J)$ are J -dimensional vectors of additive and *cis*-interaction LD scores, respectively. It
495 is important to note that, while $\boldsymbol{\chi}^2$ must be recomputed for each trait of interest, both vectors $\boldsymbol{\ell}$ and \mathbf{f}
496 only need to be constructed once per reference panel or individual-level genotypes (see next section for
497 efficient computational strategies).

498 To identify summary statistics that have significant tagged interaction effects, we test the null hy-
499 pothesis $H_0 : \sigma = NH^2(1 - \rho)/M = 0$. The **i**-LDSC software package implements the same model fitting
500 strategy as LDSC. Here, we use weighted least squares to fit the joint regression in Eq. (19) such that

$$501 \quad \hat{\sigma} = (\mathbf{f}^\top \boldsymbol{\Psi} \mathbf{f})^{-1} \mathbf{f}^\top \boldsymbol{\Psi} \boldsymbol{\chi}^2, \quad \psi_{jj} = [\ell_j \hat{\tau} + f_j \hat{\sigma} + 1]^{-2} \quad (20)$$

502 where $\boldsymbol{\Psi}$ is a $J \times J$ diagonal weight matrix with nonzero elements set to values inversely proportional to
503 the conditional variance $\mathbb{V}[\chi_j^2 | \ell_j, f_j] = \psi_{jj}^{-1}$ to adjust for both heteroscedasticity and over-estimation of
504 the summary statistics for each SNP¹⁷. Standard errors for each coefficient estimate are derived via a
505 delete-one jackknife over blocks of SNPs in the data³⁵, and we then use those standard errors to derive
506 P -values with a two-sided test (i.e., testing the alternative hypothesis $H_A : \sigma = NH^2(1 - \rho)/M \neq 0$).
507 For all analyses in this paper, we estimate proportion of phenotypic variance explained by genetic effects
508 using a sum of the coefficients $\hat{\tau} + \hat{\sigma}$ (i.e., the estimated additive component plus the additional genetic
509 variance explained by the tagged pairwise interaction effects).

510 Efficient computation of *cis*-interaction LD scores

511 In practice, *cis*-interaction LD scores in *i*-LDSC can be computed efficiently through realizing two key
512 opportunities for optimization. First, given J SNPs, the full matrix of genome-wide interaction effects
513 \mathbf{W} contains on the order of $J(J-1)/2$ total pairwise interactions. However, the correlation between
514 the genotype of the j -th SNP and the interactions where its involved (i.e., $\mathbf{x}_j^\top(\mathbf{x}_k \circ \mathbf{x}_l)$ for $l \neq j$) is
515 bound to be much larger than the correlation between the genotype of the j -th SNP \mathbf{x}_j and interactions
516 involving some other SNP (e.g., $\mathbf{x}_j^\top(\mathbf{x}_k \circ \mathbf{x}_l)$ for $k \neq j$ and $l \neq j$). To that end, we can compute the
517 *i*-LDSC score for each SNP by replacing the full \mathbf{W} matrix with a subsetting matrix \mathbf{W}_j which includes
518 only interactions involving the j -th SNP. Analogous to the original LDSC formulation¹⁷, we consider only
519 interactive SNPs within a *cis*-window proximal to the focal j -th SNP for which we are computing the
520 *i*-LDSC score. In the original LDSC model, this is based on the observation that LD decays outside of a
521 window of 1 centimorgan (cM); therefore, SNPs outside the 1 cM window centered on the j -th SNP j
522 will not significantly contribute to its LD score.

523 The second opportunity for optimization comes from the fact that the matrix of interaction effects for
524 any focal SNP, \mathbf{W}_j , does not need to be explicitly generated. Referencing Eq. (15), the *i*-LDSC scores are
525 defined as $\mathbf{x}_j^\top \mathbf{W}_j \mathbf{W}_j^\top \mathbf{x}_j / N^2$. This can be re-written as $\mathbf{x}_j^\top (\mathbf{D}_j \mathbf{X}^{(j)}) (\mathbf{D}_j \mathbf{X}^{(j)})^\top \mathbf{x}_j$, where $\mathbf{D}_j = \text{diag}(\mathbf{x}_j)$ is
526 a diagonal matrix with the j -th genotype as its nonzero elements²¹ and $\mathbf{X}^{(j)}$ denotes the subset SNPs
527 within a *cis*-window proximal to the focal j -th SNP. This means that the *i*-LDSC score for the j -th SNP
528 can be simply computed as the following

$$529 \quad f_j \approx \frac{1}{N^2} (\mathbf{x}_j^\top)^2 \mathbf{X}^{(j)} \mathbf{X}^{(j)\top} (\mathbf{x}_j)^2. \quad (21)$$

530 With these simplifications, the computational complexity of generating *i*-LDSC scores reduces to that of
531 computing LD scores — modulo a vector-by-vector Hadamard product which, for each SNP, is constant
532 factor of N (i.e., the number of genotyped individuals).

533 Coefficient estimates as determined by *cis*-interaction window size

534 When computing *cis*-interaction LD scores, the most important *decision* is choosing the number of
535 interacting SNPs to include in $\mathbf{X}^{(j)}$ (or equivalently \mathbf{W}_j for each j -th focal SNP in the calculation of f_j
536 in Eq. (21)). The *i*-LDSC framework considers different estimating windows to account for our lack of a

537 *priori* knowledge about the “correct” non-additive genetic architecture of traits. Theoretically, one could
538 follow previous work^{20,25,27,29,30,42} by considering an L -valued grid of possible SNP interaction window
539 sizes. After fitting a series of *i*-LDSC regressions with *cis*-interaction LD scores $\mathbf{f}^{(l)}$ generated under
540 the L -different window sizes, we could compute normalized importance weights using their maximized
541 likelihoods via the following

$$542 \quad \pi^{(l)} = \frac{\mathcal{L}(\boldsymbol{\ell}, \mathbf{f}^{(l)}; \hat{\boldsymbol{\beta}})}{\sum_{l'} \mathcal{L}(\boldsymbol{\ell}, \mathbf{f}^{(l')}; \hat{\boldsymbol{\beta}})}, \quad \sum_{l=1}^L \pi^{(l)} = 1. \quad (22)$$

543 As a final step in the model fitting procedure, we could then compute averaged estimates of the coefficients
544 τ and σ by marginalizing (or averaging) over the L -different grid combinations of estimating windows

$$545 \quad \hat{\tau} = \sum_{l=1}^L \pi^{(l)} \hat{\tau}^{(l)}, \quad \hat{\sigma} = \sum_{l=1}^L \pi^{(l)} \hat{\sigma}^{(l)}. \quad (23)$$

546 This final step can be viewed as an analogy to model averaging where marginal estimates are computed
547 via a weighted average using the importance weights⁴³. In the current study, we explore the utility of
548 *cis*-interaction LD scores generated with different window sizes ± 5 , ± 10 , ± 25 , and ± 50 SNPs around
549 each j -th focal SNP. In practice, we find that *cis*-interaction LD scores that are calculated using larger
550 windows lead to the most robust estimates of heritability while also not over representing the total
551 phenotypic variation explained by tagged non-additive genetic effects (see Figure S8). Therefore, unless
552 otherwise stated, we use *cis*-interaction LD scores calculated with a ± 50 SNP interaction window for all
553 simulations and real data analyses conducted in this work. For a direct comparison between choosing a
554 single window size versus the model averaging strategy described above, see Tables S1 and S2.

555 **Relationship between minor allele frequency and effect size**

556 The LDSC software computes LD scores using annotations over equally spaced minor allele frequency
557 (MAF) bins. These annotations enable the per trait relationship between the MAF and the effect size
558 of each variant in the genome to vary based on the discrete category (or MAF bin) it is placed into.
559 This additional flexibility is intended to help LDSC be more robust when estimating heritability. The
560 relationship between MAF and effect size is already implicitly encoded in the LDSC formulation since we
561 assume genotypes are normalized. When normalizing by the variance of each SNP (or equivalently its

562 MAF), we make the assumption that rare variants inherently have larger effect sizes. There exists a true
563 functional relationship between MAF and effect size which is likely to be somewhere between the two
564 extremes of (i) normalizing each SNP by its MAF and (ii) allowing the variance per SNP to be dictated
565 by its MAF.

566 Recent approaches have proposed using a single parameter α to better represent the nonlinear rela-
567 tionship between MAF and variant effect size. The main idea is that this α not only provides the same
568 additional flexibility to LDSC as the MAF-based discrete annotations, but it also empirically yields even
569 more precise heritability estimates⁴⁴. Namely, we use

$$570 \quad \ell_j(c) := \sum_k L_{jk}(\alpha) a_c(k), \quad L_{jk}(\alpha) = r_{jk}^2 \mathbb{V}[\mathbf{x}_k]^{1-\alpha} \quad (24)$$

571 where $a_c(k)$ is the annotation value for the c -th categorical bin. The α parameter is unknown in practice
572 and needs to be estimated for any given trait. While standard ranges for α can be used for heritability es-
573 timates, we use a restricted maximum likelihood (REML) based method which was recently developed³².

574 In the **i**-LDSC software, we use this α construction to handle the relationship between MAF and variant
575 effect size for two specific reasons. First, by constructing the LD scores using α , we more accurately
576 capture the variation in chi-square test statistics due to additive effects⁴⁴. Second, we note that there is
577 correlation between MAF and (i) LD scores, (ii) *cis*-interaction LD scores, and (iii) trait architecture.
578 To that end, if we do not properly condition on MAF, there becomes additional bias, and we may falsely
579 attribute some amount of variation in the chi-square test statistics to LD or the tagged interaction effects.
580 Therefore, in our formulation, we include an α term on the LD scores to condition on this effect. We
581 demonstrate in simulations that this removes the bias introduced by the relationship between MAF and
582 trait architecture, and it mitigates potential inflation of type I error rates in the **i**-LDSC test.

583 Estimation of allele frequency parameters

584 In the main text, we analyzed 25 complex traits in both the UK Biobank and BioBank Japan data sets.
585 In order to account for minor allele frequency (MAF) dependent trait architecture, we calculated α values
586 for each trait that had not been analyzed by previous studies³². The α estimates for each of the 25 traits
587 analyzed in this study are shown in Table S4. Intuitively, α parameterizes the weighting of the effects
588 of each individual variant given its frequency in the study cohort and can take on values in the range of

589 [-1,0]. More negative values of α indicate that lower frequency variants contribute more to the observed
590 variation in a trait of interest, whereas values of α closer to zero indicate that common variants contribute
591 a greater amount of variation to observed trait values.

592 We took α values for 11 traits (again see Table S4) that had previously been calculated from Schoech
593 et al.³². For the remaining 14 traits analyzed in this study, we followed the estimation protocol described
594 in the same manuscript. Specifically, using the variants passing the quality control step in our pipeline for
595 25,000 randomly selected individuals in the UK Biobank cohort, we constructed MAF-dependent genetic
596 relatedness matrices for values of $\alpha = \{-1, -0.95, -0.9, \dots, 0\}$ using the `GRM-MAF-LD` software, <https://github.com/arminschoech/GRM-MAF-LD>. We then used the GCTA software⁴⁵ to obtain heritability and
597 likelihood estimates using REML for each α -trait pairing. We then fit a trait-specific profile likelihood
598 across the range of α values and estimate the maximum likelihood value of α using a natural cubic spline.
599

600 Simulation studies

601 We used a simulation scheme to generate synthetic quantitative traits and SNP-level summary statis-
602 tics under multiple genetic architectures using real genome-wide data from individuals of self-identified
603 European ancestry in the UK Biobank. Here, we consider phenotypes that have some combination of
604 additive effects, *cis*-acting interactions, and a third source of genetic variance stemming from either gene-
605 by-environment (G×E) or gene-by-ancestry (G×Ancestry) effects. For each scenario, we select some set
606 of SNPs to be causal and assume that complex traits are generated via the following general linear model

$$607 \quad \mathbf{y} = \mathbf{X}\boldsymbol{\beta} + \mathbf{W}\boldsymbol{\theta} + \mathbf{Z}\boldsymbol{\delta} + \boldsymbol{\varepsilon}, \quad \boldsymbol{\varepsilon} \sim \mathcal{N}(\mathbf{0}, \kappa^2\mathbf{I}), \quad (25)$$

608 where \mathbf{y} is an N -dimensional vector containing all the phenotypes; \mathbf{X} is an $N \times J$ matrix of genotypes
609 encoded as 0, 1, or 2 copies of a reference allele; $\boldsymbol{\beta}$ is a J -dimensional vector of additive effect sizes for
610 each SNP; \mathbf{W} is an $N \times M$ matrix which holds all pairwise interactions between the randomly selected
611 subset of the interacting SNPs with corresponding effects $\boldsymbol{\theta}$; \mathbf{Z} is an $N \times K$ matrix of either G×E or
612 G×Ancestry interactions with coefficients $\boldsymbol{\delta}$; and $\boldsymbol{\varepsilon}$ is an N -dimensional vector of environmental noise.
613 The phenotypic variation is assumed to be $\mathbb{V}[\mathbf{y}] = 1$. All additive and interaction effect sizes for SNPs
614 are randomly drawn from independent standard Gaussian distributions and then rescaled so that they
615 explain a fixed proportion of the phenotypic variance $\mathbb{V}[\mathbf{X}\boldsymbol{\beta}] + \mathbb{V}[\mathbf{W}\boldsymbol{\theta}] + \mathbb{V}[\mathbf{Z}\boldsymbol{\delta}] = H^2$. Note that we do

616 not assume any specific correlation structure between the effect sizes β , θ , and δ . We then rescale the
617 random error term such that $\mathbb{V}[\epsilon] = (1 - H^2)$. In the main text, we compare the traditional LDSC to
618 its direct extension in **i**-LDSC. For each method, GWAS summary statistics are computed by fitting a
619 single-SNP univariate linear model via least squares where $\hat{\beta}_j = (\mathbf{x}_j^\top \mathbf{x}_j)^{-1} \mathbf{x}_j^\top \mathbf{y}$ for every $j = 1, \dots, J$ SNP
620 in the data. These effect size estimates are used to derive the chi-square test statistics $\chi_j^2 = N \hat{\beta}_j^2$. We
621 implement both LDSC and **i**-LDSC with the LD matrix $\mathbf{R} = \mathbf{X}^\top \mathbf{X} / N$ and the *cis*-interaction correlation
622 matrix $\mathbf{V} = \mathbf{X}^\top \mathbf{W} / N$ being computed using a reference panel of 489 individuals from the European
623 superpopulation (EUR) of the 1000 Genomes Project. The resulting matrices \mathbf{R} and \mathbf{V} are used to
624 compute the additive and *cis*-interaction LD scores, respectively.

625 **Polygenic simulations with *cis*-interactions.** In our first set of simulations (Figures 1-3 and S1-S8,
626 and Tables S1 and S2), we consider phenotypes with polygenic architectures that are made up of only
627 additive and *cis*-acting SNP-by-SNP interactions. Here, we begin by assuming that every SNP in the
628 genome has at least a small additive effect on the traits of interest. Next, when generating synthetic
629 traits, we assume that the additive effects make up $\rho\%$ of the heritability while the pairwise interactions
630 make up the remaining $(1 - \rho)\%$. Alternatively, the proportion of the heritability explained by additivity
631 is said to be $\mathbb{V}[\mathbf{X}\beta] = \rho H^2$, while the proportion detailed by interactions is given as $\mathbb{V}[\mathbf{W}\theta] = (1 - \rho)H^2$.
632 The setting of $\rho = 1$ represents the limiting null case for **i**-LDSC where the variation of a trait is driven
633 by solely additive effects. Here, we use the same simulation strategy used in Crawford et al.²¹ where we
634 divide the causal *cis*-interaction variants into two groups. One may view the SNPs in group #1 as being
635 the “hubs” of an interaction map. SNPs in group #2 are selected to be variants within some kilobase (kb)
636 window around each SNP in group #1. Given different parameters for the generative model in Eq. (25),
637 we simulate data mirroring a wide range of genetic architectures by toggling the following parameters:

- 638 • heritability: $H^2 = 0.3$ and 0.6 ;
- 639 • proportion of phenotypic variation that is generated by additive effects: $\rho = 0.5, 0.8$, and 1 ;
- 640 • percentage of SNPs selected to be in group #1: 1% (sparse), 5%, and 10% (polygenic);
- 641 • genomic window used to assign SNPs to group #2: ± 10 and ± 100 kilobase (kb);
- 642 • allele frequency parameter: $\alpha = -1, -0.5$, and 0 .

643 All figures and tables show the mean performances (and standard errors) across 100 simulated replicates.

644 **Polygenic simulations with gene-by-environmental effects.** In our second set of simulations
645 (Figures S9 and S12), we continue to consider phenotypes with polygenic architectures that are made
646 up of only additive and *cis*-acting SNP-by-SNP interactions; however, now we also consider each trait
647 to have contributions stemming from nonzero G×E effects. Here, both the additive and *cis*-interaction
648 effects are simulated in the same way as previously described where, for the two groups of interacting
649 variants, 10% of SNPs were selected to be in group #1 and we chose ±10 kb windows to assign SNPs to
650 group #2. To create G×E effects, we follow a simulation strategy implemented by Zhu et al.⁴⁶ and split
651 our sample population in half to emulate two subsets of individuals coming from different environments.
652 We randomly draw the effect sizes for the first environment from a standard Gaussian distribution which
653 we denote as δ_1 . We then selected an amplification coefficient w and set the effect sizes of the G×E
654 interactions in the second environment to be a scaled version of the first environment effects where
655 $\delta_2 = w\delta_1$. In this paper, we generate traits with heritability $H^2 = \{0.3, 0.6\}$ and amplification coefficients
656 set to $w = [1.1, 1.2, \dots, 2]$. For the first set of simulations, we hold the proportion of phenotypic variation
657 explained by the different genetic components constant by fixing:

- 658 • $H^2 = 0.3$: $\mathbb{V}[\mathbf{X}\beta] = 0.15$; $\mathbb{V}[\mathbf{W}\theta] = 0.075$; and $\mathbb{V}[\mathbf{Z}\delta] = 0.075$;
- 659 • $H^2 = 0.6$: $\mathbb{V}[\mathbf{X}\beta] = 0.3$; $\mathbb{V}[\mathbf{W}\theta] = 0.15$; and $\mathbb{V}[\mathbf{Z}\delta] = 0.15$;

660 where $\mathbf{Z} = [\mathbf{X}_1, \mathbf{X}_2]$ is the set of genotypes split according to environment and $\delta = [\delta_1, \delta_2]$. To test
661 the sensitivity of the *cis*-interaction LD scores to other sources of non-additive variation, we also re-
662 peated the same simulations where there were only additive and G×E effects contributing equally to
663 trait architecture:

- 664 • $H^2 = 0.3$: $\mathbb{V}[\mathbf{X}\beta] = 0.15$; $\mathbb{V}[\mathbf{W}\theta] = 0$; and $\mathbb{V}[\mathbf{Z}\delta] = 0.15$;
- 665 • $H^2 = 0.6$: $\mathbb{V}[\mathbf{X}\beta] = 0.3$; $\mathbb{V}[\mathbf{W}\theta] = 0$; and $\mathbb{V}[\mathbf{Z}\delta] = 0.3$.

666 Again all figures show the mean performances (and standard errors) across 100 simulated replicates.

667 **Polygenic simulations with gene-by-ancestry effects.** In our third set of simulations (Figures S10,
668 S11, S13, and S14), we consider phenotypes with polygenic architectures that are made up of additive, *cis*-
669 interactions, and G×Ancestry effects. Here, we follow Sohaail et al.⁴⁷ and first run a matrix decomposition
670 on the individual-level genotype matrix $\mathbf{X} = \mathbf{U}\mathbf{Q}^\top$ where \mathbf{U} is a unitary $N \times K$ score matrix, \mathbf{Q} is a

671 $K \times J$ loadings matrix, and K represents the number of (predetermined) principal components (PCs).
672 To generate $G \times$ Ancestry interactions, we then create the matrix $\mathbf{Z}_k = \mathbf{X}\mathbf{q}_k$ where \mathbf{q}_k is a J -dimensional
673 vector of SNP loadings for the k -th principal component. In this paper, we generate traits with heritability
674 $H^2 = \{0.3, 0.6\}$ and interaction effects taken over $k = 1, \dots, 10$ principal components. For the first set of
675 simulations, we hold the proportion of phenotypic variation explained by the different genetic components
676 constant by fixing:

677 • $H^2 = 0.3$: $\mathbb{V}[\mathbf{X}\boldsymbol{\beta}] = 0.15$; $\mathbb{V}[\mathbf{W}\boldsymbol{\theta}] = 0.075$; and $\mathbb{V}[\mathbf{Z}\boldsymbol{\delta}] = 0.075$;

678 • $H^2 = 0.6$: $\mathbb{V}[\mathbf{X}\boldsymbol{\beta}] = 0.3$; $\mathbb{V}[\mathbf{W}\boldsymbol{\theta}] = 0.15$; and $\mathbb{V}[\mathbf{Z}\boldsymbol{\delta}] = 0.15$;

679 To test the sensitivity of the *cis*-interaction LD scores to other sources of non-additive variation, we also
680 repeated the same simulations where there were only additive and $G \times E$ effects contributing equally to
681 trait architecture:

682 • $H^2 = 0.3$: $\mathbb{V}[\mathbf{X}\boldsymbol{\beta}] = 0.15$; $\mathbb{V}[\mathbf{W}\boldsymbol{\theta}] = 0$; and $\mathbb{V}[\mathbf{Z}\boldsymbol{\delta}] = 0.15$;

683 • $H^2 = 0.6$: $\mathbb{V}[\mathbf{X}\boldsymbol{\beta}] = 0.3$; $\mathbb{V}[\mathbf{W}\boldsymbol{\theta}] = 0$; and $\mathbb{V}[\mathbf{Z}\boldsymbol{\delta}] = 0.3$.

684 Note that, for each case, we generate summary statistics in two ways: (*i*) including the top 10 PCs as
685 covariates in the marginal linear model to correct for population structure and (*ii*) not correcting for any
686 population structure. Again all figures show the mean performances (and standard errors) across 100
687 simulated replicates.

688 **Sparse simulation study design.** In our final set of simulations, we consider phenotypes with sparse
689 architectures²⁰ (Figure S15). Here, traits were simulated with solely additive effects such that $\mathbb{V}[\mathbf{X}\boldsymbol{\beta}] =$
690 H^2 , but this time only variants with the top or bottom $\{1, 5, 10, 25, 50, 100\}$ percentile of LD scores
691 were given nonzero coefficients. We once again generate traits with heritability $H^2 = \{0.3, 0.6\}$. We
692 also want to note that, in each of these specific analyses, synthetic trait architectures were generated
693 using all UK Biobank genotyped variants that passed initial preprocessing and quality control (see next
694 section). Since not all of these SNPs are HapMap3 SNPs, some variants were omitted from the LDSC and
695 *i*-LDSC regression. Overall, as shown in the main text with results taken over 100 replicates, breaking the
696 assumed relationship between LD scores and chi-squared statistics (i.e., that they are generally positively
697 correlated) led to unbounded estimates of heritability in all but the (more polygenic) scenario when 100%
698 of SNPs contributed to phenotypic variation.

699 Preprocessing for the UK Biobank and BioBank Japan

700 In order to apply the i-LDSC framework to 25 continuous traits the UK Biobank⁴⁸, we first down-
701 loaded genotype data for 488,377 individuals in the UK Biobank using the `ukbgene` tool (<https://biobank.ctsu.ox.ac.uk/crystal/download.cgi>) and converted the genotypes using the provided
702 `ukbconv` tool (<https://biobank.ctsu.ox.ac.uk/crystal/refer.cgi?id=149660>). Phenotype data
703 for the 25 continuous traits were also downloaded for those same individuals using the `ukbgene` tool.
704 Individuals identified by the UK Biobank as having high heterozygosity, excessive relatedness, or aneu-
705 ploidy were removed (1,550 individuals). After separating individuals into self-identified ancestral cohorts
706 using data field `21000`, unrelated individuals were selected by randomly choosing an individual from
707 each pair of related individuals. This resulted in $N = 349,469$ white British individuals to be included
708 in our analysis. We downloaded imputed SNP data from the UK Biobank for all remaining individuals
709 and removed SNPs with an information score below 0.8. Information scores for each SNP are provided
710 by the UK Biobank (<http://biobank.ctsu.ox.ac.uk/crystal/refer.cgi?id=1967>).

712 Quality control for the remaining genotyped and imputed variants was then performed on each co-
713 hort separately using the following steps. All structural variants were first removed, leaving only single
714 nucleotide polymorphisms (SNPs) in the genotype data. Next, all AT/CG SNPs were removed to avoid
715 possible confounding due to sequencing errors. Then, SNPs with minor allele frequency less than 1%
716 were removed using the PLINK 2.0⁴⁹ command `--maf 0.01`. We then removed all SNPs found to be
717 out of Hardy-Weinberg equilibrium, using the PLINK `--hwe 0.000001` flag to remove all SNPs with a
718 Fisher's exact test P -value $> 10^{-6}$. Finally, all SNPs with missingness greater than 1% were removed
719 using the PLINK `--mind 0.01` flag.

720 We then performed a genome-wide association study (GWAS) for each trait in the UK Biobank on
721 the remaining 8,981,412 SNPs. SNP-level GWAS effect sizes were calculated using PLINK and the `--glm`
722 flag⁴⁹. Age, sex, and the first twenty principal components were included as covariates for all traits
723 analyzed⁴⁷. Principal component analysis was performed using FlashPCA 2.0⁵⁰ on a set of independent
724 markers derived separately for each ancestry cohort using the PLINK command `--indep-pairwise 100 10 0.1`.
725 Using the parameters `--indep-pairwise` removes all SNPs that have a pairwise correlation above 0.1
726 within a 100 SNP window, then slides forward in increments of ten SNPs genome-wide.

727 In order to analyze data from BioBank Japan, we downloaded publicly available GWAS summary
728 statistics for the 25 traits listed in Table S5 from <http://jenger.riken.jp/en/result>. Summary

729 statistics used age, sex, and the first ten principal components as confounders in the initial GWAS study.
730 We then used individuals from the East Asian (EAS) superpopulation from the 1000 Genomes Project
731 Phase 3 to calculate paired LDSC and *i*-LDSC scores from a reference panel. We pruned the reference
732 panel using the PLINK command `--indep-pairwise 100 10 0.5` to limit the computational time of
733 calculating scores⁴⁹. This resulted in reference scores for 1,164,666 SNPs that are included on the *i*-LDSC
734 GitHub repository (see URLs). Using summary statistics from BioBank Japan, with scores calculated
735 from the EAS population in the 1000 Genomes, we obtained *i*-LDSC heritability estimates for each of the
736 25 traits.

737 **Data and software availability**

738 Source code and tutorials for implementing interaction-LD score regression via the *i*-LDSC package are
739 written in Python and are publicly available online at <https://github.com/lcrawlab/i-LDSC>. Files
740 of LD scores, *cis*-interaction LD scores, and GWAS summary statistics used for our analyses of the UK
741 Biobank and BioBank Japan can be downloaded from the Harvard Dataverse (<https://dataverse.harvard.edu/dataset.xhtml?persistentId=doi:10.7910/DVN/W6MA8J&faces-redirect=true>). All
742 software for the traditional and stratified LD score regression framework with LDSC and *s*-LDSC were
743 fit using the default settings, unless otherwise stated in the main text. Source code for these approaches
744 was downloaded from <https://github.com/bulik/ldsc>. When applying *s*-LDSC, we used 97 func-
745 tional annotations from Gazal et al.³⁴ to estimate heritability. Data from the UK Biobank Resource⁴⁸
746 (<https://www.ukbiobank.ac.uk>) was made available under Application Numbers 14649 and 22419.
747 Data can be accessed by direct application to the UK Biobank.
748

749 **Figures and Tables**

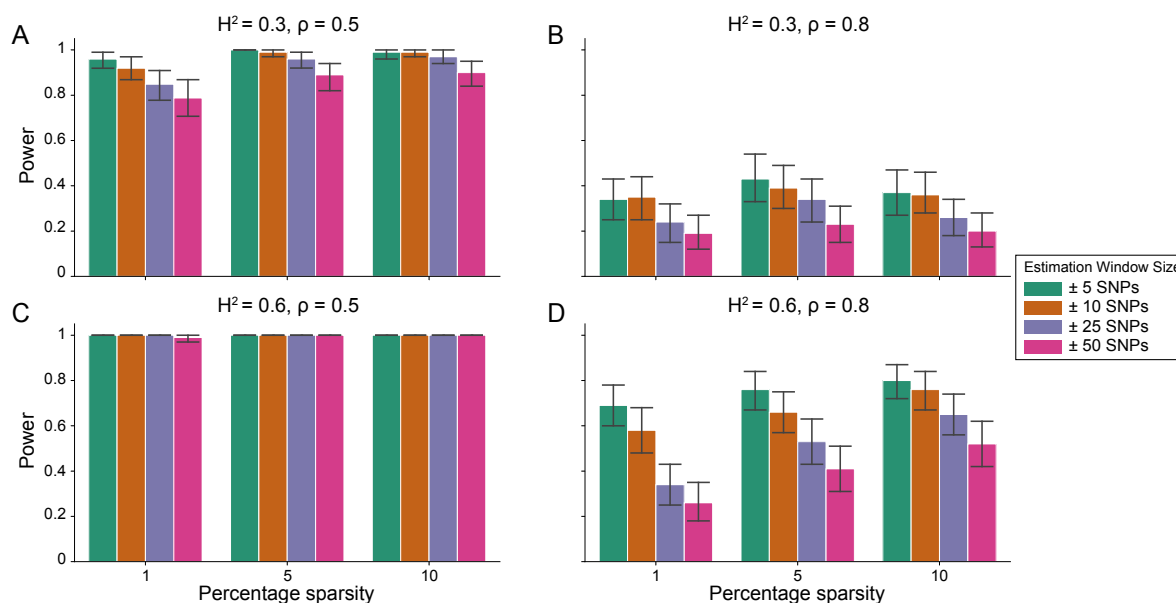


Figure 1. Power of the *i*-LDSC framework to detect tagged non-additive genetic effects on simulated data. Synthetic trait architecture was simulated using real genotype data from individuals of self-identified European ancestry in the UK Biobank. All SNPs were considered to have at least an additive effect (i.e., creating a polygenic trait architecture). Next, we randomly select two groups of interacting variants and divide them into two groups. The group #1 SNPs are chosen to be 1%, 5%, and 10% of the total number of SNPs genome-wide (see the x-axis in each panel). These interact with the group #2 SNPs which are selected to be variants within a ± 10 kilobase (kb) window around each SNP in group #1. Coefficients for additive and interaction effects were simulated with no minor allele frequency dependency $\alpha = 0$ (see Materials and Methods). Panels (A) and (B) are results with simulations using a heritability $H^2 = 0.3$, while panels (C) and (D) were generated with $H^2 = 0.6$. We also varied the proportion of heritability contributed by additive effects to (A, C) $\rho = 0.5$ and (B, D) $\rho = 0.8$, respectively. Here, we are blind to the parameter settings used in generative model and run *i*-LDSC while computing the *cis*-interaction LD scores using different estimating windows of ± 5 (green), ± 10 (orange), ± 25 (purple), and ± 50 (pink) SNPs. Results are based on 100 simulations per parameter combination and the horizontal bars represent standard errors. Generally, the performance of *i*-LDSC increases with larger heritability and lower proportions of additive variation. Note that LDSC is not shown here because it does not search for tagged interaction effects in summary statistics. Similar plots for a range of α values and generative interacting SNP window sizes are shown in Figures S1-S5.

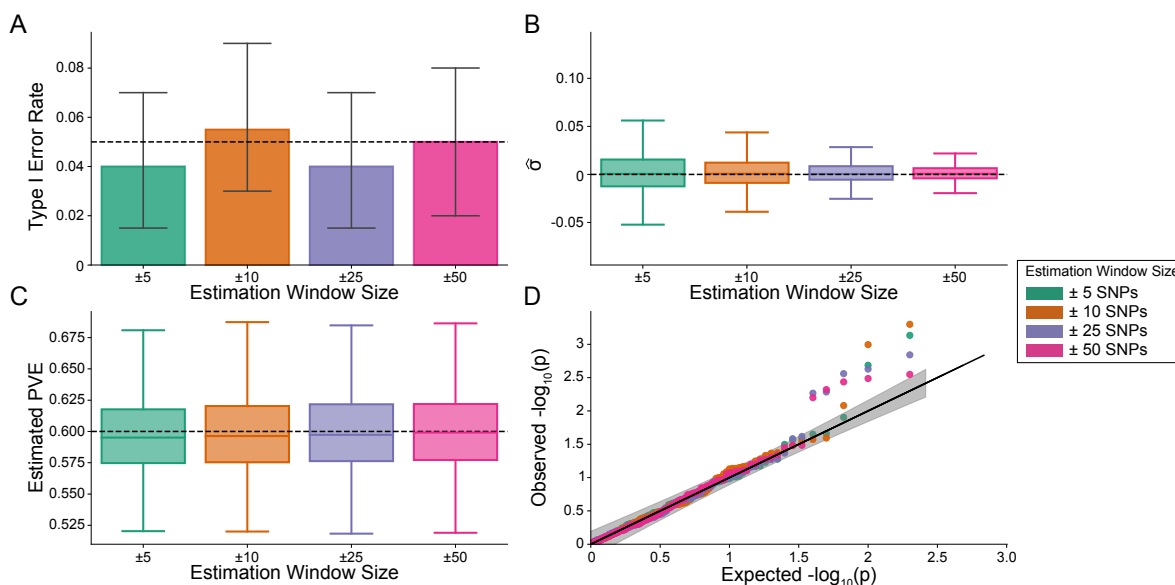


Figure 2. The *i*-LDSC framework is well-calibrated under the null hypothesis and does not identify evidence of tagged non-additive effects when polygenic traits are generated by only additive effects. In these simulations, synthetic trait architecture is made up of only additive genetic variation (i.e., $\rho = 1$). Coefficients for additive and interaction effects were simulated with no minor allele frequency dependency $\alpha = 0$ (see Materials and Methods). Here, we are blind to the parameter settings used in generative model and run *i*-LDSC while computing the *cis*-interaction LD scores using different estimating windows of ± 5 (green), ± 10 (orange), ± 25 (purple), and ± 50 (pink) SNPs. **(A)** Mean type I error rate using the *i*-LDSC framework across an array of estimation window sizes for the *cis*-interaction LD scores. This is determined by assessing the P -value of the *cis*-interaction coefficient (σ) in the *i*-LDSC regression model and checking whether $P < 0.05$. **(B)** Estimates of the *cis*-interaction coefficient (σ). Since traits were simulated with only additive effects, these estimates should be centered around zero. **(C)** Estimates of the proportions of phenotypic variance explained (PVE) by genetic effects (i.e., estimated heritability) where the true additive variance is set to $H^2\rho = 0.6$. **(D)** QQ-plot of the P -values for the *cis*-interaction coefficient (σ) in *i*-LDSC. Results are based on 100 simulations per parameter combination and the horizontal bars represent standard errors. Similar plots for a range of α values and generative interacting SNP window sizes are shown in Figures S6-S7.

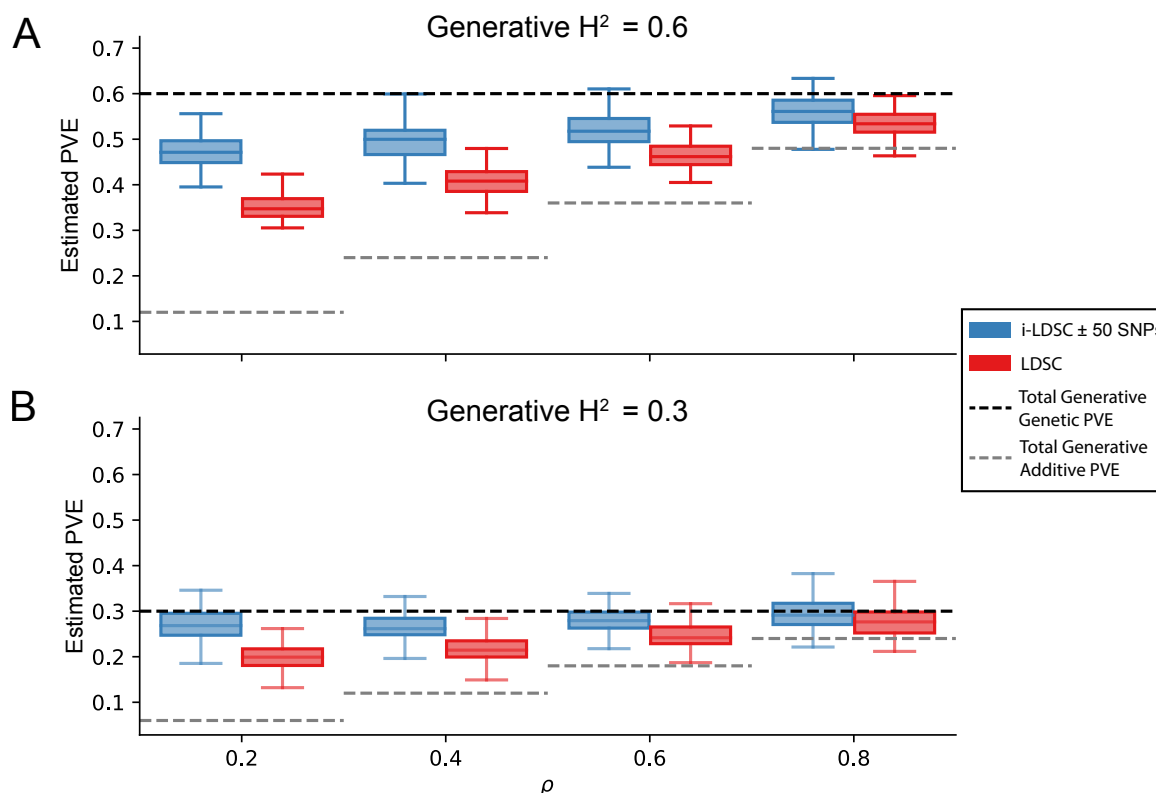


Figure 3. i-LDSC robustly and accurately estimates the proportions of phenotypic variance explained (PVE) by genetic effects (i.e., estimated heritability) in simulations in polygenic traits, compared to LDSC, due to our accounting for interaction effects tagged in additive GWAS summary statistics. Synthetic trait architecture was simulated using real genotype data from individuals of self-identified European ancestry in the UK Biobank (Materials and Methods). All SNPs were considered to have at least an additive effect (i.e., creating a polygenic trait architecture). Next, we randomly select two groups of interacting variants and divide them into two groups. The group #1 SNPs are chosen to be 10% of the total number of SNPs genome-wide. These interact with the group #2 SNPs which are selected to be variants within a ± 100 kilobase (kb) window around each SNP in group #1. Coefficients for additive and interaction effects were simulated with no minor allele frequency dependency $\alpha = 0$ (see Materials and Methods). Here, we assume a heritability (A) $H^2 = 0.3$ or (B) $H^2 = 0.6$ (marked by the black dotted lines, respectively), and we vary the proportion contributed by additive effects with $\rho = \{0.2, 0.4, 0.6, 0.8\}$. The grey dotted lines represent the total contribution of additive effects in the generative model for the synthetic traits ($H^2\rho$). i-LDSC outperforms LDSC in recovering heritability across each scenario. Results are based on 100 simulations per parameter combination. i-LDSC estimates of heritability partitioned by estimation *cis*-interaction window are shown in Figure S8. The mean absolute error between the true H^2 value and the estimates produced by i-LDSC and LDSC are shown in Table S1 and S2, respectively.

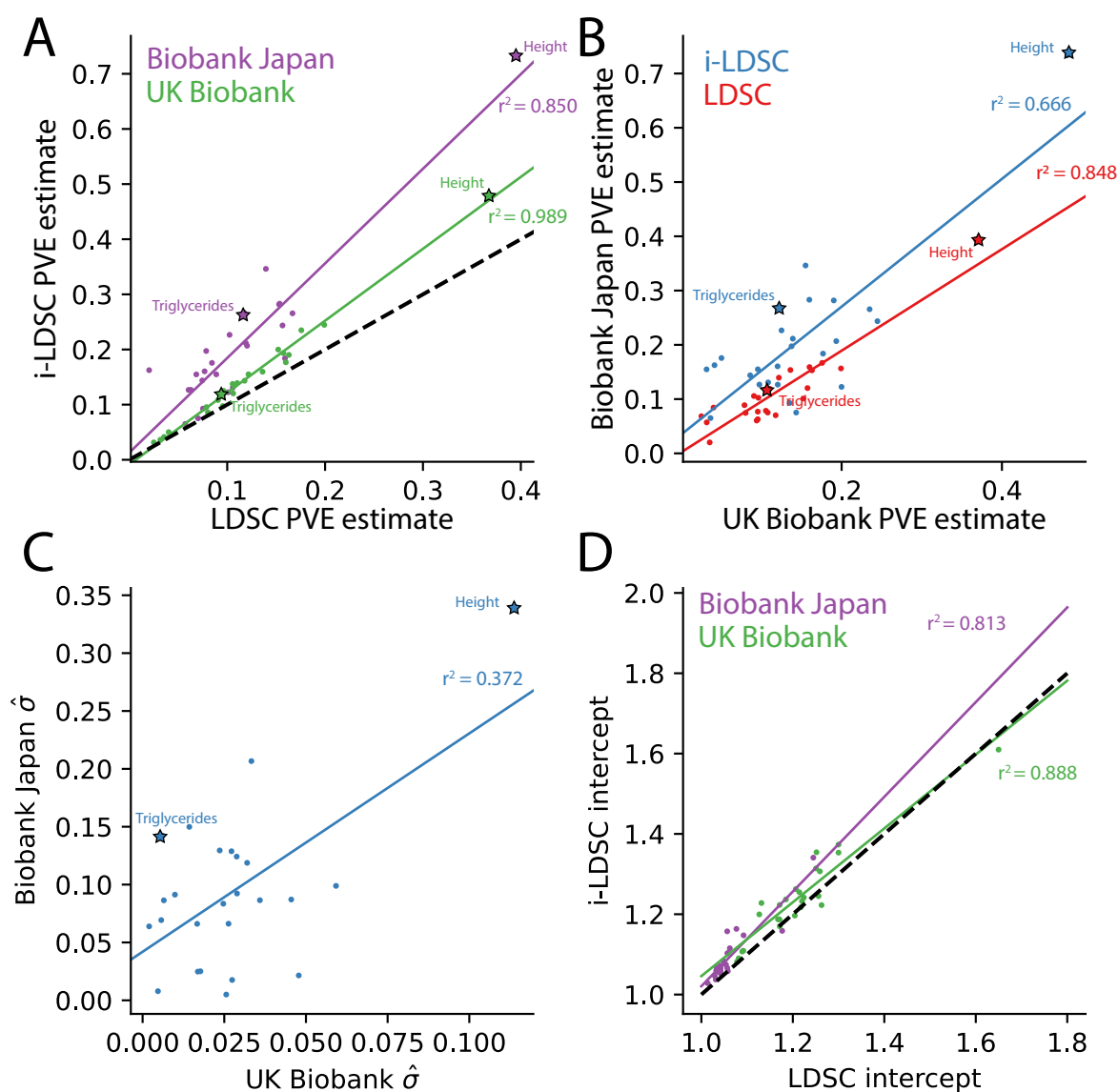


Figure 4. The i-LDSC framework recovers heritability and provides estimates of tagged *cis*-interactions in GWAS summary statistics (σ) for 25 quantitative traits in the UK Biobank and BioBank Japan. (A) In both the UK Biobank (green) and BioBank Japan (purple), estimates of phenotypic variance explained (PVE) by genetic effects from i-LDSC and LDSC are highly correlated for 25 different complex traits. The Spearman correlation coefficient between heritability estimates from LDSC and i-LDSC for the UK Biobank and BioBank Japan are $r^2 = 0.989$ and $r^2 = 0.850$, respectively. The $y = x$ dotted line represents the values at which estimates from both approaches are the same. (B) PVE estimates from the UK Biobank are better correlated with those from the BioBank Japan across 25 traits using LDSC (Spearman $r^2 = 0.848$) than i-LDSC (Spearman $r^2 = 0.666$). (C) i-LDSC estimates of the phenotypic variation explained by tagged non-additive genetic effects using the *cis*-interaction LD score (i.e., estimates of σ) between traits in the UK Biobank and BioBank Japan (Spearman $r^2 = 0.372$). (D) Intercept estimates between i-LDSC and LDSC regression models are highly correlated in the UK Biobank (Spearman $r^2 = 0.888$, slope = 0.919) and BioBank Japan (Spearman $r^2 = 0.813$, slope = 1.179). When height, an outlier in our UK Biobank analysis is omitted, the slope of the UK Biobank intercept line is closer to that of the BioBank Japan (UKB slope with no outlier = 1.070). Note that the heritability estimates displayed in panels (A) and (B), and P -values corresponding to panel (C), are given in Table 1.

Trait	UKB (LDSC)	UKB (i-LDSC)	UKB $\hat{\sigma}$	UKB <i>P</i> -value	BBJ (LDSC)	BBJ (i-LDSC)	BBJ $\hat{\sigma}$	BBJ <i>P</i> -value
Basophil	0.0250	0.0315	0.0065	1.572×10^{-12}	0.0684	0.1548	0.0864	0.025
BMI	0.1757	0.2349	0.0592	3.083×10^{-84}	0.1667	0.2656	0.0989	2.438×10^{-18}
Cholesterol	0.0954	0.0974	0.0020	1.821×10^{-16}	0.0629	0.1268	0.0639	2.740×10^{-4}
CRP	0.0354	0.0414	0.0060	9.845×10^{-12}	0.0202	0.1625	0.1423	0.020
DBP	0.0940	0.1203	0.0263	1.118×10^{-65}	0.0605	0.1267	0.0662	1.675×10^{-7}
EGFR	0.1521	0.1999	0.0478	1.187×10^{-46}	0.1010	0.1225	0.0215	4.232×10^{-5}
Eosinophil	0.1055	0.1375	0.0320	1.230×10^{-18}	0.0785	0.1973	0.1188	0.001
HBA1C	0.0906	0.1083	0.0177	1.578×10^{-26}	0.1057	0.1308	0.0251	0.031
HDL*	0.1599	0.1768	0.0169	9.636×10^{-37}	0.1590	0.1838	0.0248	0.081
Height	0.3675	0.4815	0.1140	1.038×10^{-64}	0.2340	0.3941	0.1601	7.433×10^{-33}
Hematocrit	0.1078	0.1352	0.0274	2.479×10^{-25}	0.0752	0.0928	0.0176	3.689×10^{-5}
Hemoglobin	0.1177	0.1433	0.0256	4.284×10^{-27}	0.0702	0.0752	0.0050	9.037×10^{-4}
LDL	0.0802	0.0859	0.0057	5.087×10^{-13}	0.0745	0.1438	0.0693	0.018
Lymphocyte	0.0402	0.0501	0.0099	4.906×10^{-19}	0.0844	0.1757	0.0913	5.479×10^{-5}
MCH	0.1361	0.1597	0.0236	1.785×10^{-25}	0.1536	0.2831	0.1295	1.042×10^{-5}
MCHC	0.0317	0.0364	0.0047	3.730×10^{-12}	0.0571	0.0650	0.0079	0.027
MCV	0.1630	0.1902	0.0272	1.180×10^{-29}	0.1530	0.2818	0.1288	1.042×10^{-5}
Monocyte	0.0788	0.0955	0.0167	5.257×10^{-18}	0.0888	0.1549	0.0661	0.004
Neutrophil	0.1102	0.1391	0.0289	1.777×10^{-33}	0.1191	0.2114	0.0923	5.050×10^{-5}
Platelet	0.1992	0.2447	0.0455	2.303×10^{-37}	0.1565	0.2436	0.0871	7.724×10^{-9}
RBC	0.1574	0.1933	0.0359	3.292×10^{-31}	0.1203	0.2068	0.0865	5.972×10^{-8}
SBP	0.0954	0.1201	0.0247	8.660×10^{-75}	0.0769	0.1604	0.0835	9.075×10^{-10}
Triglycerides*	0.1061	0.1204	0.0143	1.410×10^{-26}	0.1171	0.2670	0.1499	0.110
Urate	0.1217	0.1550	0.0333	9.642×10^{-38}	0.1395	0.3462	0.2067	0.015
WBC	0.0962	0.1250	0.0288	9.866×10^{-34}	0.1024	0.2266	0.1242	1.346×10^{-8}

Table 1. i-LDSC heritability estimates and *P*-values highlighting statistically significant contributions of tagged non-additive genetic effects for 25 traits in the UK Biobank and BioBank Japan. Here, LDSC heritability estimates are included as a baseline. The difference between the approaches is that the i-LDSC heritability estimates include proportions of phenotypic variation that are explained by tagged non-additive variation (see columns with estimates $\hat{\sigma}$). Note that all 25 traits analyzed in the UK Biobank and 23 of the 25 traits analyzed in BioBank Japan have a statistically significant amount of tagged non-additive genetic effects as detected by the *cis*-interaction LD score ($P < 0.05$). The two traits without significant tagged non-additive genetic effects in BioBank Japan were HDL ($P = 0.081$) and Triglyceride ($P = 0.110$). These traits are indicated by *. The i-LDSC *P*-values are related to the estimates of the σ coefficients which are also displayed in Figure 4.

References

- 750 1. Brendan K Bulik-Sullivan, Po-Ru Loh, Hilary K Finucane, Stephan Ripke, Jian Yang, Nick Pat-
751 terson, Mark J Daly, Alkes L Price, and Benjamin M Neale. Ld score regression distinguishes
752 confounding from polygenicity in genome-wide association studies. *Nature genetics*, 47(3):291–
753 295, 2015.
- 754
755 2. Brendan Bulik-Sullivan, Hilary K Finucane, Verner Anttila, Alexander Gusev, Felix R Day, Po-
756 Ru Loh, Laramie Duncan, John R B Perry, Nick Patterson, Elise B Robinson, Mark J Daly,
757 Alkes L Price, Benjamin M Neale, ReproGen Consortium, Psychiatric Genomics Consortium, and
758 Genetic Consortium for Anorexia Nervosa of the Wellcome Trust Case Control Consortium 3. An
759 atlas of genetic correlations across human diseases and traits. *Nature Genetics*, 47(11):1236–1241,
760 2015. doi: 10.1038/ng.3406. URL <https://doi.org/10.1038/ng.3406>.
- 761 3. Huwenbo Shi, Gleb Kichaev, and Bogdan Pasaniuc. Contrasting the genetic architecture of 30
762 complex traits from summary association data. *The American Journal of Human Genetics*, 99(1):
763 139–153, 2016.
- 764 4. Noah Zaitlen, Peter Kraft, Nick Patterson, Bogdan Pasaniuc, Gaurav Bhatia, Samuela Pollack, and
765 Alkes L. Price. Using extended genealogy to estimate components of heritability for 23 quantitative
766 and dichotomous traits. *PLOS Genetics*, 9(5):1–11, 2013. doi: 10.1371/journal.pgen.1003520. URL
767 <https://doi.org/10.1371/journal.pgen.1003520>.
- 768 5. Tinca J C Polderman, Beben Benyamin, Christiaan A de Leeuw, Patrick F Sullivan, Arjen van
769 Bochoven, Peter M Visscher, and Danielle Posthuma. Meta-analysis of the heritability of human
770 traits based on fifty years of twin studies. *Nature Genetics*, 47(7):702–709, 2015. doi: 10.1038/ng.
771 3285. URL <https://doi.org/10.1038/ng.3285>.
- 772 6. Kangcheng Hou, Kathryn S. Burch, Arunabha Majumdar, Huwenbo Shi, Nicholas Mancuso, Yue
773 Wu, Sriram Sankararaman, and Bogdan Pasaniuc. Accurate estimation of snp-heritability from
774 biobank-scale data irrespective of genetic architecture. *Nature Genetics*, 51(8):1244–1251, 2019.
775 doi: 10.1038/s41588-019-0465-0. URL <https://doi.org/10.1038/s41588-019-0465-0>.
- 776 7. Ali Pazokitoroudi, Yue Wu, Kathryn S. Burch, Kangcheng Hou, Aaron Zhou, Bogdan Pasaniuc,
777 and Sriram Sankararaman. Efficient variance components analysis across millions of genomes.

- 778 Nature Communications, 11(1):4020, 2020. doi: 10.1038/s41467-020-17576-9. URL <https://doi.org/10.1038/s41467-020-17576-9>.
- 779
- 780 8. Loic Yengo, Julia Sidorenko, Kathryn E Kemper, Zhili Zheng, Andrew R Wood, Michael N Weedon,
781 Timothy M Frayling, Joel Hirschhorn, Jian Yang, Peter M Visscher, et al. Meta-analysis of genome-
782 wide association studies for height and body mass index in 700000 individuals of european ancestry.
783 Human molecular genetics, 27(20):3641–3649, 2018.
- 784 9. Doug Speed and David J Balding. Sumher better estimates the snp heritability of complex traits
785 from summary statistics. Nature genetics, 51(2):277–284, 2019.
- 786 10. Shuang Song, Wei Jiang, Yiliang Zhang, Lin Hou, and Hongyu Zhao. Leveraging ld eigenvalue
787 regression to improve the estimation of snp heritability and confounding inflation. The American
788 Journal of Human Genetics, 2022.
- 789 11. Duncan S Palmer, Wei Zhou, Liam Abbott, Emilie M Wigdor, Nikolas Baya, Claire Churchhouse,
790 Cotton Seed, Tim Poterba, Daniel King, Masahiro Kanai, et al. Analysis of genetic dominance in
791 the uk biobank. Science, 379(6639):1341–1348, 2023.
- 792 12. Tsz Fung Chan, Xinyue Rui, David V. Conti, Myriam Fornage, Mariaelisa Graff, Jeffrey Haessler,
793 Christopher Haiman, Heather M. Highland, Su Yon Jung, Eimear Kenny, Charles Kooperberg,
794 Loic Le Marchand, Kari E. North, Ran Tao, Genevieve Wojcik, Christopher R. Gignoux, PAGE
795 Consortium, Charleston W. K. Chiang, and Nicholas Mancuso. Estimating heritability explained
796 by local ancestry and evaluating stratification bias in admixture mapping from summary statistics.
797 bioRxiv, page 2023.04.10.536252, 2023. doi: 10.1101/2023.04.10.536252. URL <http://biorxiv.org/content/early/2023/04/18/2023.04.10.536252.abstract>.
- 798
- 799 13. Zheng Ning, Yudi Pawitan, and Xia Shen. High-definition likelihood inference of genetic cor-
800 relations across human complex traits. Nature Genetics, 52(8):859–864, 2020. doi: 10.1038/
801 s41588-020-0653-y. URL <https://doi.org/10.1038/s41588-020-0653-y>.
- 802 14. Yiliang Zhang, Qiongshi Lu, Yixuan Ye, Kunling Huang, Wei Liu, Yuchang Wu, Xiaoyuan Zhong,
803 Boyang Li, Zhaolong Yu, Brittany G Travers, Donna M Werling, James J Li, and Hongyu Zhao.
804 Supergnova: local genetic correlation analysis reveals heterogeneous etiologic sharing of complex

- traits. Genome Biol, 22(1):262, 2021. ISSN 1474-760X (Electronic); 1474-7596 (Print); 1474-7596 (Linking). doi: 10.1186/s13059-021-02478-w.
15. Roshni A. Patel, Shaila A. Musharoff, Jeffrey P. Spence, Harold Pimentel, Catherine Tcheandjieu, Hakhamanesh Mostafavi, Nasa Sinnott-Armstrong, Shoa L. Clarke, Courtney J. Smith, Peter P. Durda, Kent D. Taylor, Russell Tracy, Yongmei Liu, W. Craig Johnson, Francois Aguet, Kristin G. Ardlie, Stacey Gabriel, Josh Smith, Deborah A. Nickerson, Stephen S. Rich, Jerome I. Rotter, Philip S. Tsao, Themistocles L. Assimes, and Jonathan K. Pritchard. Genetic interactions drive heterogeneity in causal variant effect sizes for gene expression and complex traits. The American Journal of Human Genetics, 2022. doi: 10.1016/j.ajhg.2022.05.014. URL <https://doi.org/10.1016/j.ajhg.2022.05.014>.
16. Evan E. Eichler, Jonathan Flint, Greg Gibson, Augustine Kong, Suzanne M. Leal, Jason H. Moore, and Joseph H. Nadeau. Missing heritability and strategies for finding the underlying causes of complex disease. Nature Reviews Genetics, 11(6):446–450, 2010. doi: 10.1038/nrg2809. URL <https://doi.org/10.1038/nrg2809>.
17. Brendan K Bulik-Sullivan, Po-Ru Loh, Hilary K Finucane, Stephan Ripke, Jian Yang, Schizophrenia Working Group of the Psychiatric Genomics Consortium, Nick Patterson, Mark J Daly, Alkes L Price, and Benjamin M Neale. Ld score regression distinguishes confounding from polygenicity in genome-wide association studies. Nat Genet, 47:291–295, 2015. URL <http://dx.doi.org/10.1038/ng.3211>.
18. Jian Yang, Beben Benyamin, Brian P McEvoy, Scott Gordon, Anjali K Henders, Dale R Nyholt, Pamela A Madden, Andrew C Heath, Nicholas G Martin, and Grant W Montgomery. Common snps explain a large proportion of the heritability for human height. Nat Genet, 42(7):565, 2010.
19. Michael C Wu, Seunggeun Lee, Tianxi Cai, Yun Li, Michael Boehnke, and Xihong Lin. Rare-variant association testing for sequencing data with the sequence kernel association test. Am J Hum Genet, 89(1):82–93, 2011. ISSN 1537-6605 (Electronic); 0002-9297 (Linking). doi: 10.1016/j.ajhg.2011.05.029.
20. Xiang Zhou, Peter Carbonetto, and Matthew Stephens. Polygenic modeling with Bayesian sparse linear mixed models. PLoS Genet, 9(2):e1003264, 2013.

- 833 21. Lorin Crawford, Ping Zeng, Sayan Mukherjee, and Xiang Zhou. Detecting epistasis with the
834 marginal epistasis test in genetic mapping studies of quantitative traits. *PLoS Genet*, 13(7):
835 e1006869, 2017. URL <https://doi.org/10.1371/journal.pgen.1006869>.
- 836 22. William G. Hill, Michael E. Goddard, and Peter M. Visscher. Data and theory point to mainly
837 additive genetic variance for complex traits. *PLOS Genetics*, 4(2):1–10, 2008. doi: 10.1371/journal.
838 pgen.1000008. URL <https://doi.org/10.1371/journal.pgen.1000008>.
- 839 23. Farhad Hormozdiari, Emrah Kostem, Eun Yong Kang, Bogdan Pasaniuc, and Eleazar Eskin. Iden-
840 tifying causal variants at loci with multiple signals of association. *Genetics*, 198(2):497–508, 2014.
841 doi: 10.1534/genetics.114.167908. URL <https://pubmed.ncbi.nlm.nih.gov/25104515>.
- 842 24. Priyanka Nakka, Benjamin J Raphael, and Sohini Ramachandran. Gene and Network Analysis
843 of Common Variants Reveals Novel Associations in Multiple Complex Diseases. *Genetics*, 204(2):
844 783–798, 10 2016. ISSN 1943-2631. doi: 10.1534/genetics.116.188391. URL [https://doi.org/](https://doi.org/10.1534/genetics.116.188391)
845 [10.1534/genetics.116.188391](https://doi.org/10.1534/genetics.116.188391).
- 846 25. Xiang Zhu and Matthew Stephens. Bayesian large-scale multiple regression with summary statistics
847 from genome-wide association studies. *Ann Appl Stat*, 11(3):1561–1592, 2017. doi: 10.1214/
848 17-AOAS1046. URL <https://projecteuclid.org:443/euclid.aos/1507168840>.
- 849 26. Yan Zhang, Guanghao Qi, Ju-Hyun Park, and Nilanjan Chatterjee. Estimation of complex effect-
850 size distributions using summary-level statistics from genome-wide association studies across 32
851 complex traits. *Nat Genet*, 50(9):1318–1326, 2018.
- 852 27. Xiang Zhu and Matthew Stephens. Large-scale genome-wide enrichment analyses identify new
853 trait-associated genes and pathways across 31 human phenotypes. *Nat Comm*, 9(1):4361, 2018.
- 854 28. Wei Cheng, Sohini Ramachandran, and Lorin Crawford. Estimation of non-null snp effect size
855 distributions enables the detection of enriched genes underlying complex traits. *PLoS Genet*, 16
856 (6):e1008855, 2020. URL <https://doi.org/10.1371/journal.pgen.1008855>.
- 857 29. Pinar Demetci, Wei Cheng, Gregory Darnell, Xiang Zhou, Sohini Ramachandran, and Lorin
858 Crawford. Multi-scale inference of genetic trait architecture using biologically annotated neu-

- 859 ral networks. *PLOS Genetics*, 17(8):1–53, 2021. doi: 10.1371/journal.pgen.1009754. URL
860 <https://doi.org/10.1371/journal.pgen.1009754>.
- 861 30. Yongtao Guan and Matthew Stephens. Bayesian variable selection regression for genome-wide
862 association studies and other large-scale problems. *Ann Appl Stat*, 5(3):1780–1815, 2011. doi:
863 10.1214/11-AOAS455. URL <https://projecteuclid.org:443/euclid.aoas/1318514285>.
- 864 31. Ronald Aylmer Fisher. *The genetical theory of natural selection: a complete variorum edition*.
865 Oxford University Press, 1999. ISBN 0198504403.
- 866 32. Armin P Schoech, Daniel M Jordan, Po-Ru Loh, Steven Gazal, Luke J O’Connor, Daniel J Bal-
867 ick, Pier F Palamara, Hilary K Finucane, Shamil R Sunyaev, and Alkes L Price. Quantification
868 of frequency-dependent genetic architectures in 25 uk biobank traits reveals action of negative
869 selection. *Nature communications*, 10(1):1–10, 2019.
- 870 33. Yabo Li, Hyosuk Cho, Fan Wang, Oriol Canela-Xandri, Chunyan Luo, Konrad Rawlik, Stephen
871 Archacki, Chengqi Xu, Albert Tenesa, Qiuyun Chen, et al. Statistical and functional studies
872 identify epistasis of cardiovascular risk genomic variants from genome-wide association studies.
873 *Journal of the American Heart Association*, 9(7):e014146, 2020.
- 874 34. Steven Gazal, Hilary K Finucane, Nicholas A Furlotte, Po-Ru Loh, Pier Francesco Palamara,
875 Xuanyao Liu, Armin Schoech, Brendan Bulik-Sullivan, Benjamin M Neale, Alexander Gusev, et al.
876 Linkage disequilibrium-dependent architecture of human complex traits shows action of negative
877 selection. *Nature genetics*, 49(10):1421–1427, 2017.
- 878 35. Hilary K Finucane, Brendan Bulik-Sullivan, Alexander Gusev, Gosia Trynka, Yakir Reshef, Po-Ru
879 Loh, Verner Anttila, Han Xu, Chongzhi Zang, Kyle Farh, Stephan Ripke, Felix R Day, Shaun
880 Purcell, Eli Stahl, Sara Lindstrom, John R B Perry, Yukinori Okada, Soumya Raychaudhuri,
881 Mark J Daly, Nick Patterson, Benjamin M Neale, and Alkes L Price. Partitioning heritability
882 by functional annotation using genome-wide association summary statistics. *Nat Genet*, 47(11):
883 1228–1235, 2015. ISSN 1546-1718 (Electronic); 1061-4036 (Print); 1061-4036 (Linking). doi: 10.
884 1038/ng.3404.
- 885 36. Daniel Runcie, Hao Cheng, and Lorin Crawford. Mega-scale linear mixed models for ge-
886 nomic predictions with thousands of traits. *bioRxiv*, page 2020.05.26.116814, 2020. doi:

- 887 10.1101/2020.05.26.116814. URL [http://biorxiv.org/content/early/2020/05/29/2020.05.](http://biorxiv.org/content/early/2020/05/29/2020.05.26.116814.abstract)
888 [26.116814.abstract](http://biorxiv.org/content/early/2020/05/29/2020.05.26.116814.abstract).
- 889 37. Julian Stamp, Alan DenAdel, Daniel Weinreich, and Lorin Crawford. Leveraging the genetic
890 correlation between traits improves the detection of epistasis in genome-wide association studies.
891 bioRxiv, page 2022.11.30.518547, 2022. doi: 10.1101/2022.11.30.518547. URL [http://biorxiv.](http://biorxiv.org/content/early/2022/12/01/2022.11.30.518547.abstract)
892 [org/content/early/2022/12/01/2022.11.30.518547.abstract](http://biorxiv.org/content/early/2022/12/01/2022.11.30.518547.abstract).
- 893 38. Sahin Naqvi, Yoeri Sleyp, Hanne Hoskens, Karlijne Indencleef, Jeffrey P. Spence, Rose Bruffaerts,
894 Ahmed Radwan, Ryan J. Eller, Stephen Richmond, Mark D. Shriver, John R. Shaffer, Seth M.
895 Weinberg, Susan Walsh, James Thompson, Jonathan K. Pritchard, Stefan Sunaert, Hilde Peeters,
896 Joanna Wysocka, and Peter Claes. Shared heritability of human face and brain shape. Nature
897 Genetics, 53(6):830–839, 2021. doi: 10.1038/s41588-021-00827-w. URL [https://doi.org/10.](https://doi.org/10.1038/s41588-021-00827-w)
898 [1038/s41588-021-00827-w](https://doi.org/10.1038/s41588-021-00827-w).
- 899 39. Yong Jiang and Jochen C. Reif. Modeling epistasis in genomic selection. Genetics, 201:759–768,
900 2015.
- 901 40. Farhad Hormozdiari, Martijn van de Bunt, Ayellet V. Segrè, Xiao Li, Jong Wha J. Joo, Michael
902 Bilow, Jae Hoon Sul, Sriram Sankararaman, Bogdan Pasaniuc, and Eleazar Eskin. Colocalization
903 of GWAS and eQTL signals detects target genes. Am J Hum Genet, 99(6):1245–1260, 2016. doi:
904 [10.1016/j.ajhg.2016.10.003](https://doi.org/10.1016/j.ajhg.2016.10.003). URL <https://doi.org/10.1016/j.ajhg.2016.10.003>.
- 905 41. L. Isserlis. On a formula for the product-moment coefficient of any order of a normal frequency
906 distribution in any number of variables. Biometrika, 12(1-2):134–139, 1918. ISSN 0006-3444. doi:
907 [10.1093/biomet/12.1-2.134](https://doi.org/10.1093/biomet/12.1-2.134). URL <https://doi.org/10.1093/biomet/12.1-2.134>.
- 908 42. Peter Carbonetto and Matthew Stephens. Scalable variational inference for bayesian variable
909 selection in regression, and its accuracy in genetic association studies. Bayesian Anal, 7(1):73–108,
910 2012.
- 911 43. Jennifer A. Hoeting, David Madigan, Adrian E. Raftery, and Chris T. Volinsky. Bayesian model
912 averaging: a tutorial (with comments by m. clyde, david draper and e. i. george, and a rejoinder
913 by the authors. Statist Sci, 14(4):382–417, 1999. doi: 10.1214/ss/1009212519. URL [https:](https://projecteuclid.org:443/euclid.ss/1009212519)
914 [//projecteuclid.org:443/euclid.ss/1009212519](https://projecteuclid.org:443/euclid.ss/1009212519).

- 915 44. Shadi Zabad, Aaron P Ragsdale, Rosie Sun, Yue Li, and Simon Gravel. Assumptions about
916 frequency-dependent architectures of complex traits bias measures of functional enrichment.
917 Genetic epidemiology, 45(6):621–632, 2021.
- 918 45. Jian Yang, S Hong Lee, Michael E Goddard, and Peter M Visscher. Gcta: a tool for genome-
919 wide complex trait analysis. Am J Hum Genet, 88(1):76–82, 2011. ISSN 1537-6605 (Electronic);
920 0002-9297 (Print); 0002-9297 (Linking). doi: 10.1016/j.ajhg.2010.11.011.
- 921 46. Carrie Zhu, Matthew J. Ming, Jared M. Cole, Michael D. Edge, Mark Kirkpatrick, and Arbel
922 Harpak. Amplification is the primary mode of gene-by-sex interaction in complex human traits.
923 Cell Genomics, 3(100297), 2023. doi: 10.1016/j.xgen.2023.100297. URL [https://doi.org/10.](https://doi.org/10.1016/j.xgen.2023.100297)
924 [1016/j.xgen.2023.100297](https://doi.org/10.1016/j.xgen.2023.100297).
- 925 47. Mashaal Sohail, Robert M Maier, Andrea Ganna, Alex Bloemendal, Alicia R Martin, Michael C
926 Turchin, Charleston WK Chiang, Joel Hirschhorn, Mark J Daly, Nick Patterson, et al. Polygenic
927 adaptation on height is overestimated due to uncorrected stratification in genome-wide association
928 studies. Elife, 8:e39702, 2019.
- 929 48. Clare Bycroft, Colin Freeman, Desislava Petkova, Gavin Band, Lloyd T. Elliott, Kevin Sharp,
930 Allan Motyer, Damjan Vukcevic, Olivier Delaneau, Jared O’Connell, Adrian Cortes, Samantha
931 Welsh, Alan Young, Mark Effingham, Gil McVean, Stephen Leslie, Naomi Allen, Peter Donnelly,
932 and Jonathan Marchini. The uk biobank resource with deep phenotyping and genomic data.
933 Nature, 562(7726):203–209, 2018. doi: 10.1038/s41586-018-0579-z. URL [https://doi.org/10.](https://doi.org/10.1038/s41586-018-0579-z)
934 [1038/s41586-018-0579-z](https://doi.org/10.1038/s41586-018-0579-z).
- 935 49. Christopher C Chang, Carson C Chow, Laurent CAM Tellier, Shashaank Vattikuti, Shaun M
936 Purcell, and James J Lee. Second-generation plink: rising to the challenge of larger and richer
937 datasets. Gigascience, 4(1):s13742–015, 2015.
- 938 50. Gad Abraham, Yixuan Qiu, and Michael Inouye. Flashpca2: principal component analysis of
939 biobank-scale genotype datasets. Bioinformatics, 2017.
- 940 51. Masahiro Kanai, Masato Akiyama, Atsushi Takahashi, Nana Matoba, Yukihide Momozawa,
941 Masashi Ikeda, Nakao Iwata, Shiro Ikegawa, Makoto Hirata, Koichi Matsuda, et al. Genetic anal-

- 942 ysis of quantitative traits in the japanese population links cell types to complex human diseases.
943 Nature genetics, 50(3):390–400, 2018.
- 944 52. Masato Akiyama, Yukinori Okada, Masahiro Kanai, Atsushi Takahashi, Yukihide Momozawa,
945 Masashi Ikeda, Nakao Iwata, Shiro Ikegawa, Makoto Hirata, Koichi Matsuda, et al. Genome-wide
946 association study identifies 112 new loci for body mass index in the japanese population. Nature
947 genetics, 49(10):1458, 2017.
- 948 53. Masato Akiyama, Kazuyoshi Ishigaki, Saori Sakaue, Yukihide Momozawa, Momoko Horikoshi,
949 Makoto Hirata, Koichi Matsuda, Shiro Ikegawa, Atsushi Takahashi, Masahiro Kanai, et al. Char-
950 acterizing rare and low-frequency height-associated variants in the japanese population. Nature
951 communications, 10(1):1–11, 2019.